SC5202.23FR

Copy No. 15

GROWTH OF HgCdTe BY MODIFIED MOLECULAR BEAM EPITAXY

FINAL REPORT FOR THE PERIOD
February 11, 1979 through March 31, 1983

CONTRACT NO. MDA903-79-C-0188
DARPA ORDER NO. 3704

Prepared for

Defense Advanced Research Projects Agency
1400 Wilson Boulevard
Arlington, VA 22209

Principal Investigators
J.T. Cheung, H. Sankur
(805) 498-4545

DECEMBER 1983

Approved for public release; distribution unlimited

This research was sponsored by the Defense Advanced Research Projects Agency under DARPA Order No. 3704; Contract No. MDA903-79-C-0188; Monitored by the Defense Supply Service.

The views and conclusions contained in this document are those of the author and should not be interpreted as necessarily representing the official policies, either expressed or implied, of the Defense Advanced Research Projects Agency or the United States Government.

Rockwell International
Science Center

UNCLASSIFIED

SECURITY CLASSIFICATION OF THIS PAGE (When Data Entered)

REPORT DOCUMENTATION PAGE	READ DISTRUCTIONS BEFORE COMPLETING FORM
1. REPORT NUMBER	2. GOVT ACCESSION NO. AD-A137243	3. RECIPIENT'S CATALOG NUMBER
4. TITLE (and Subtitle) GROWTH OF HgCdTe BY MODIFIED MOLECULAR BEAM EPITAXY	5. TYPE OF REPORT & PERIOD COVERED Final Report for the Period 02/11/79 thru 03/31/83
	6. PERFORMING ORG. REPORT NUMBER SC5202.23FR
7. AUTHOR(s) J.T. Cheung, H. Sankur	8. CONTRACT OR GRANT NUMBER(s) MDA903-79-C-0188
9. PERFORMING ORGANIZATION NAME AND ADDRESS Rockwell International Science Center 1049 Camino Dos Rios Thousand Oaks, CA 91360	10. PROGRAM ELEMENT, PROJECT, TASK AREA & WORK UNIT NUMBERS DARPA Order No. 3704 Program Code No. 9D10 Prog. Element Code: 61101E
11. CONTROLLING OFFICE NAME AND ADDRESS Defense Advanced Research Projects Agency 1400 Wilson Boulevard Arlington, VA 22209	12. REPORT DATE December 1983
	13. NUMBER OF PAGES 73
14. MONITORING AGENCY NAME & ADDRESS(if different from Controlling Office)	15. SECURITY CLASS. (of this report) Unclassified
	15a. DECLASSIFICATION/DOWNGRADING SCHEDULE

16. DISTRIBUTION STATEMENT (of this Report)

Approved for public release; distribution unlimited.

17. DISTRIBUTION STATEMENT (of the abstract entered in Block 20, if different from Report)

18. SUPPLEMENTARY NOTES

19. KEY WORDS (Continue on reverse side if necessary and identify by block number)

Thin film, epitaxy, laser assisted deposition, HgCdTe, CdTe, GaAs, ZnO, piezoelectric, surface acoustic wave devices

.0001

Micrometers

20. ABSTRACT (Continue on reverse side if necessary and identify by block number)

Laser assisted deposition was applied successfully to thin film growth of three materials: HgCdTe, CdTe and ZnO.

For HgCdTe, congruent evaporation was induced by pulsed laser irradiation. Epitaxial $Hg_{0.7}Cd_{0.3}Te$ layers up to 15 μm thick were grown on (111) CdTe substrates at 120°C in 10^{-4} Torr of Hg backpressure from a single evaporation source. Materials were characterized structurally and electrically. The as-grown layers were n-type. After 410°C annealing, they

Cont'd

DD FORM 1 JAN 73 1473 EDITION OF 1 NOV 65 IS OBSOLETE

UNCLASSIFIED

SECURITY CLASSIFICATION OF THIS PAGE (When Data Entered)

were converted to p-type. n+/p implanted photodiodes were demonstrated.

Very high quality (111) CdTe/(100)GaAs heteroepitaxy was demonstrated. The growth rate was as high as 12 μm/hr. The layers were characterized with x-ray, photoluminescence, UV reflectance and transmission electron microscopy and found to have very high crystalline quality.

ZnO films were grown on a large variety of substrates using a pulsed CO_2 laser. The substrate temperatures were only 250°C, the films were highly oriented and uniform. They were also piezoelectric. Surface and acoustic wave transducers were demonstrated. Coupling coefficient K^2 was found to be 0.005.

TABLE OF CONTENTS

LIST OF FIGURES

LIST OF FIGURES

LIST OF FIGURES

FOREWORD

The main objective of this research program was the development of a novel thin film deposition technique known as laser assisted deposition and annealing (LADA) and its applications to various materials. The program was divided into two phases: the first phase covered the work performed from February 1979 to February 1981, with the second phase covering the period May 1981 through April 1983. There was a time lag of three months between these two phases.

Work performed during the first two years concentrated on the initial development of this technique and involved $Hg_{1-x}Cd_xTe$ growth exclusively. Accomplishments during this period include the design and construction of a LADA apparatus, and experimental study on the evaporation-deposition mechanism of $Hg_{1-x}Cd_xTe$ during irradiation with high power laser pulses. Results showed that evaporation of HgCdTe under such conditions is congruent and dissociative. Work performed during this period laid the technical foundation and established the potential of LADA as a versatile thin film growth technique.

During the second phase, the work on HgCdTe was continued with emphasis on optimization of HgCdTe growth conditions and on the hetero-epitaxial growth of CdTe on foreign substrates. The combination of these tasks can result in an all LADA process of HgCdTe layers grown on foreign substrates. In addition, a new task for making piezoelectric ZnO film was added. A new LADA apparatus was built and devoted to this new task. The LADA apparatus demonstrated high quality LADA grown ZnO films and fabricated ultrasonic transducers. This report documents the progress made during this phase of the program. The results include HgCdTe epitaxy, CdTe on GaAs heteroepitaxy and ZnO thin film growth.

The program was sponsored by DARPA and monitored by Dr. R. Reynolds. Their support and encouragements are acknowledged. We are also grateful to the technical support from D. Matthews, J. Pasko and J. Bajaj, as well as collaboration with Dr. T. Magee (characterization by TEM) and Dr. E. Motamedi (ZnO SAW device fabrication and testing).

1.0 INTRODUCTION

The new technique is appropriately named LADA (Laser Assisted Deposition and Annealing), because it uses a high energy laser as an external power source for evaporating source materials as well as annealing the as-grown films in situ. In this work, laser radiation was only used for material evaporation. In the past, there have been several reports[1] on the use of laser evaporation to deposit thin films. The deposited materials ranged from refractory metals, semiconductors and even organic compounds. However, there was a lack of persistent effort to pursue the development of this technique. Our work takes a systematic approach to optimize the process and make it competitive with the more conventional techniques such as molecular beam epitaxy, sputtering, etc. The work is divided into the growth of HgCdTe (and CdTe) and ZnO films.

During the last few years, HgCdTe epitaxy has become the focal point of growth efforts for this important infrared (IR) detection material. LADA has gradually been accepted as a promising vacuum deposition technique. Because of the difficulties associated with noncongruent evaporation of HgCdTe and Hg re-evaporation from the surface of as-deposited layers, HgCdTe epitaxy by means of any conventional vacuum deposition technique is not straightforward. In our last report, we demonstrated that LADA can overcome these problems. In this continual effort, we concentrate on optimizing growth conditions[2] and the effect of various growth parameters. We have successfully grown p-type $Hg_{0.7}Cd_{0.3}Te$ epitaxial films on CdTe substrate.[3] Ion implanted photodiodes on these materials have been demonstrated.

Another major objective is to search for an alternative material to substitute for CdTe as substrate for HgCdTe growth. Because of its metallurgical compatibility with HgCdTe, CdTe becomes a natural choice for substrate material. CdTe, however, is difficult to grow, mechanically fragile, and exhibits low thermal conductivity. Indeed, the availability of high quality CdTe is generally recognized as the most severe impediment to the

development of HgCdTe epitaxial growth technology. An immediate solution to this can be provided by growing epitaxial CdTe films on alternative substrates which could then serve as nucleating surfaces for subsequent HgCdTe growth. In this work, we have extensively studied the heteroepitaxial growth of CdTe on GaAs with very successful results.[4] GaAs is chosen since high quality, large area wafers are readily available and it is transparent in IR regions up to 18 μm wavelengths. Despite the large lattice mismatch ($\Delta a/a = 14.6\%$), the <111> CdTe films grown on (100) GaAs show very high crystallinity. Coupling the efforts of HgCdTe/CdTe and CdTe/GaAs growth by LADA, the ultimate goal of growing HgCdTe epitaxial layers on a foreign substrate such as GaAs becomes a reality.

The LADA technique has also been extended to other materials such as ZnO. It is a wide bandgap (3.3 eV) compound that has very high piezoelectric coefficient, exhibits birefringence, Pockel cell E-O effect, and is transparent in the visible and IR regions. Its applications can be found in many areas such as heterojunction solar cells, optical waveguides, etc. The most important application of ZnO is perhaps surface acoustic wave (SAW) devices, based on its piezoelectric properties. ZnO films have been grown by CVD,[5] MOCVD,[6] close space vapor transport,[7] and various forms of sputtering.[8] Thus far, only films made by sputtering are found to be piezoelectric. LADA is an attractive alternative to sputtering. The laser power is delivered in a form of high power pulses causing flash evaporation condition. The response time is nearly instantaneous allowing for precise adjustment. Low growth temperature is also expected due to the high impinging energy of the evaporated species. In this work, we have successfully grown c-axis oriented ZnO films which are highly resistive.[9] Growth temperature ranges from 50-450°C. Effects of various post annealing conditions and in situ doping were studied. Finally, the LADA-grown ZnO films are piezoelectric and ultrasonic transducers have been fabricated and characterized.

This report will describe the progress of these tasks in detail. Section 3.0 gives experimental details on the apparatus, growth conditions,

post-growth treatments and characterizations. Results and discussions are presented in Section 4.0. Section 5.0 contains concluding remarks and points out the uniqueness of LADA as compared to other techniques and its future research and applications. Section 6.0 gives a list of publications as a result of this contract and other works related to LADA.

2.0 EXPERIMENTAL

2.1 LADA Apparatus

There are two LADA setups for ZnO and HgCdTe studies, respectively. The HgCdTe LADA apparatus has been greatly modified since its completion in the first phase of the program. The ZnO apparatus was constructed during this reporting period.

2.1.1 HgCdTe LADA Apparatus

Figure 1 shows the schematic configuration of a LADA apparatus. The main chamber is a 12 in. I.D. all metal unit. It is pumped by a Hg diffusion pump backed with a freon cooled baffle and a liquid nitrogen trap. The choice of Hg diffusion pump is based on the ease of operation and low impurity level since the pumping fluid, Hg, is already a constituent of the HgCdTe system.

The substrate holder is made of molybdenum. The temperature can be regulated to within ± 0.5°C up to 800°C. The holder area is 1.5 in. diameter. The source holder consists of two separate platforms mounted on a rotary feed-through. This adds flexibility to the system for multiple layers of growth. The source to substrate distance is 3 in.

A pool of Hg is connected to the main chamber through a valve. By throttling pumping speed, the Hg backpressure in the system can be maintained from 6×10^{-4} Torr to less than 10^{-6} Torr. The ultimate pressure in the chamber is 7×10^{-8} Torr.

The high energy laser is a Nd:YAG unit with radiation at 1.06 μm wavelength; maximum cw multimode output is 100 W. The laser is equipped with an acousto-optical Q-switch for pulsed operation. The beam can be scanned over the source by a pair of galvanometrically controlled mirrors. Laser power density is adjusted by focusing or defocusing the beam or by direct adjustment of the laser output power. A $LiIO_3$ crystal frequency doubler was used to convert part of the radiation to 530 nm. The conversion efficiency was less than 1%.

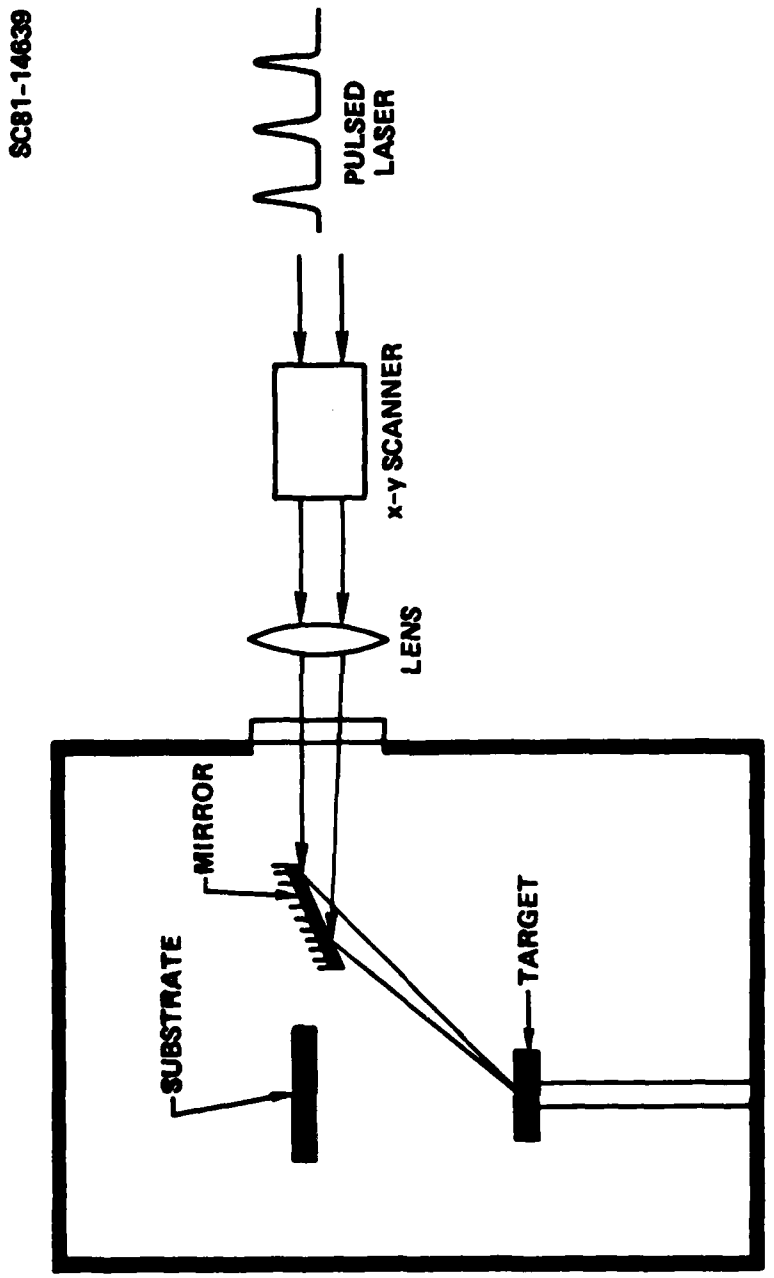

Fig. 1 LADA apparatus for HgCdTe and CdTe.

2.1.2 ZnO LADA Apparatus

The ZnO LADA apparatus is shown in Fig. 2. It consists of a stainless steel vacuum chamber, pumped by a Perkin Elmer 8 in. cryopump and liquid nitrogen cold shrouds. The ultimate pressure attainable is 2×10^{-8} Torr range. The vacuum system is also equipped with controlled leak valves and vacuum port throttle to achieve any desired background pressure within 10^{-6}-10^{-2} Torr range. The latter and high-voltage feedthroughs allow ac or dc glow discharge to be set in any gas ambient. The growing film thickness is measured by quartz crystal thickness monitors and by optically monitoring the monochromatic reflectance from the film. The optical reflectance apparatus shown in Fig. 2 consists of a He-Ne laser and laser line filter. The sensitivity of the optical thickness monitoring system is about 50Å.

The ZnO evaporation sources are mounted on rotary pedestals. The substrate holder is made of molybdenum for cleanliness and can be heated to 500°C. It is also possible to bias the substrate with respect to gas plasma in the system. The substrates are mounted using liquid Ga as a heat conducting medium, therefore minimizing any discrepancy between the measured substrate holder temperature and the actual substrate temperature. The typical substrate-source distance was 6 in. but can be varied to achieve better film thickness uniformity.

The power for evaporation derives from an 80 W CO_2 laser which was operated in pulsed or cw modes. The 10.6 μm wavelength laser beam was focussed with an AR coated ZnSe lens and scanned across the evaporation target by scanning mirrors. A NaCl window was used to transmit the laser beam into the vacuum chamber. The window was protected from the evaporant flux by shields and by the use of an internally heated molybdenum mirror to deflect the laser beam onto the source material. This configuration eliminates the line of sight between the window and the source material, thus preventing condensation of evaporants onto the window surface. The heating of the mirror allowed most of the Zn to reevaporate from the mirror surface maintaining the

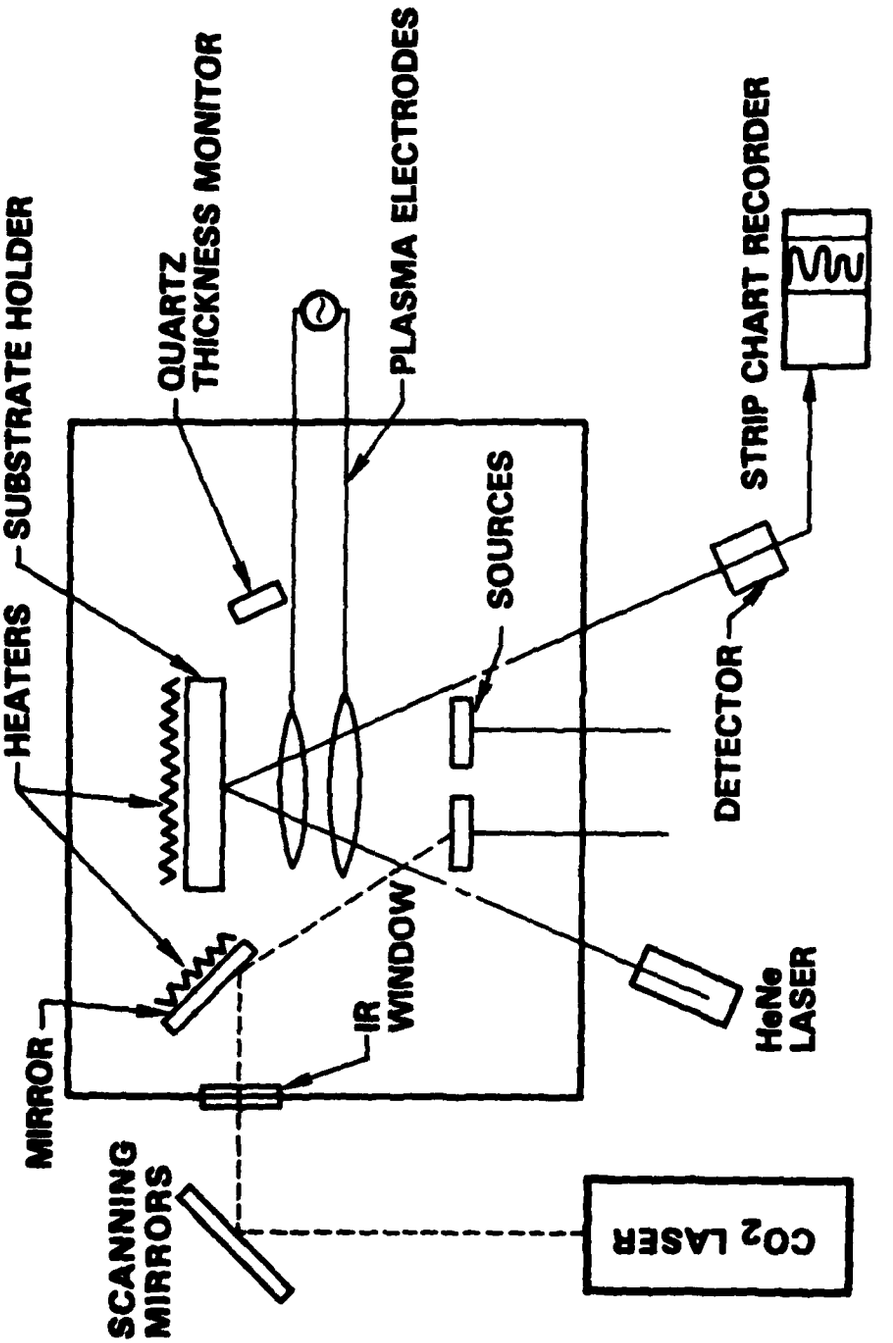

Fig. 2 LADA apparatus for ZnO.

initial high reflectance of the mirror for the CO_2 laser beam. The advantages of using molybdenum as mirror material are that it is oxidation resistant and does not react with zinc.

2.2 Film Growth Procedures

This section describes growth procedures and conditions of three types of thin films, (1) HgCdTe/CdTe, (2) CdTe/GaAs and (3) ZnO on various substrates.

2.2.1 HgCdTe/CdTe

(111)A oriented CdTe substrates were used. They were degreased and etched in 1% bromine/methanol solution for 1 min prior to loading. The substrates were mounted on a molybdenum holder wetted with indium for uniform thermal contact. After the vacuum reached a low range of 10^{-7} Torr, CdTe was then heated to 300°C briefly and cooled down to a lower temperature for HgCdTe growth.

Bulk $Hg_{1-x}Cd_xTe$ ($x = 0.3$ and $x = 0.2$) crystals from New England Research Center were used as target sources. They were cut to pieces 1 in. long and 1/2 in. diameter and were placed on rotatable holders. Before deposition the target source was rastered with focused laser beam for 30 min in order to "scrub" off any surface contamination. Deposition took place in 2×10^{-4} Torr Hg backpressure. The growth rate was adjusted by varying the laser beam power density and scan rate. Films from 5 μm to 15 μm thick were grown. Film quality depends strongly on the laser condition. 50 KHz pulse frequency, 200 ns pulse duration, and power density from 5×10^5 W/cm^2 to 5×10^7 W/cm^2 have been used. Post annealing was carried out in Hg overpressure at both 210°C and 410°C. Typical annealing time was 4 h.

The films were characterized by optical transmission, x-ray diffraction and Hall measurement at different temperatures. Impurity analyses were carried out for some samples by secondary ion mass spectroscopy (SIMS). On some samples the C-V characteristics of MIS capacitors were also measured.

Two other types of target material for producing HgCdTe film were also studied briefly. One approach was to press pellets from $(HgTe)_{1-x}(CdTe)_x$ powder mixture while the other was to use separate HgTe and CdTe sources and rapidly scan the laser beam over them to cause alloy depositing on the substrate. These two approaches offer tuning capability of the alloy composition.

2.2.2 CdTe/GaAs

CdTe/GaAs heteroepitaxy has been extensively studied. Undoped, semi-insulating (100) GaAs wafers were etched in $H_2SO_4/H_2O_2/H_2O$ solution and mounted on a substrate holder. This surface treatment leaves a thin layer of native oxide which can be removed by heating the substrate to 570°C in vacuo. Undoped CdTe crystals were used as target source. Just like HgCdTe, the CdTe target was "scrubbed" by rastering laser beam to remove surface contaminants. The growth temperature was 350°C. However, this was the reading of a thermocouple inserted into the molybdenum block; the actual temperature of the substrate was probably lower. Growth rate varied from 3 μm/h to 12 μm/h and film thickness varied from 3 μm to 15 μm.

Films were characterized by x-ray diffraction, UV reflection, photoluminescence, and transmission electron microscopy (TEM). TEM work was performed by T. Magee of the Advanced Research and Application Corporation.

2.2.3 ZnO

Before detailed descriptions on the growth procedure, we shall justify the use of LADA technique for growing ZnO films. ZnO is one of the most widely studied wide-gap semiconductors. Numerous growth techniques can be classified into three categories. First is chemical vapor deposition which includes close space vapor transport and low pressure metal-organic CVD[5] (MOCVD).[6] ZnO films from these processes exhibit good crystallinity. The main disadvantages are the high substrate temperature, poor crystallinity and poor surface morphology of the films which are usually rough and faceted. The second technique is sputtering[8] among which magnetron sputtering is the most

promising. ZnO films prepared by this technique are considered as state-of-the-art. Only ZnO films produced by sputtering are piezoelectric. It is interesting to note that throughout an extensive literature search, we could not find any work on direct evaporation of ZnO either by resistive heating or by E-beam heating, although these techniques are perhaps the simplest and most well developed forms of vacuum deposition. A possible reason is the decomposition and noncongruent evaporation of ZnO at elevated temperatures. This problem was avoided by pulsed heating with high power radiation from a CO_2 laser in the LADA approach.

We have tried a wide range of experimental conditions in order to understand the kinetics of evaporation and deposition process as well as optimization of film quality. We have found that the film properties were determined by many variables including laser parameters (power density and scan rate), choice of source materials, substrates, growth temperature and ambient environment.

Three kinds of ZnO targets were used: (1) sintered ZnO pellets purchased from MRC, (2) 99.9999% pure ZnO powder cold-pressed 1/2 in. diameter pellets and (3) ZnO mixed with 1% $Li_2O \cdot H_2O$ in solution, dried and pressed into pellets. The focused laser beam scanned across the pellet while the latter rotated on its axis or the laser beam was scanned in a raster fashion. This helped achieve thickness uniformity of the growing film over a distance of 3-5 cm, because the pellet acted like a 1/2 in. diameter area source rather than a point source.

Substrates used in this work included Si[(100), (111)], GaAs[(100), (111)], quartz, Corning 7059 glass, gold and titanium films. Substrates were mounted on molybdenum holder wetted with Ga for uniform thermal contact. Substrate temperatures were varied from 100-400°C. Evaporation rate was controlled from 0.1Å - 10Å/s by the laser power density and scan rate. Typical film thicknesses were about 1 μm. Experiments were carried out in high vacuum ($< 10^{-6}$ Torr), in a partial pressure of O_2 (10^{-2} - 10^{-4} Torr) and in O_2 glow discharge. Effects of the growth ambient were studied. In addition to the

studies of growth conditions, some films were also subjected to post annealing in oxygen or air ambient in order to improve their qualities.

ZnO films were characterized by x-ray diffraction for structural properties, by ellipsometry, reflectance and transmittance spectroscopy for optical properties, and by electrical conductivity measurements. Some films are piezoelectric. Ultrasonic transducers have also been demonstrated.

Interaction between the laser radiation and ZnO target was also studied by mass spectroscopic analysis of the evaporant plume with a residual gas analyzer. Information from this study was used to understand the evaporation and deposition mechanism.

3.0 RESULTS AND DISCUSSION

3.1 HgCdTe/CdTe

3.1.1 Optimization of Growth Conditions

The important growth parameters are laser power density, growth rate, substrate temperature and the amount of Hg backpressure. They will be discussed separately.

3.1.1.1 Effect of Hg Backpressure

HgCdTe could evaporate congruently under pulsed laser irradiation. However, due to the low sticking coefficient of Hg, the presence of a Hg backpressure (p_{Hg}) during the evaporation-deposition process was essential to compensate for Hg loss in order to form stoichiometric films. In this study, a more systematic study has been carried out.

In a series of experiments, we studied the film composition as a function of P_{Hg}. A piece of $Hg_{0.7}Cd_{0.3}$ Te crystal was used as target material. The deposition rate was 1.2 μm/h and the substrate was CdTe <III>A at room temperature. The Hg backpressure, P_{Hg}, ranging from 10^{-6} to 2×10^{-4} Torr, was controlled by throttling a valve connecting a pool of mercury to the main chamber. The pressure readings were taken directly from an ionization gauge without any correction for the ionization efficiency of mercury.

Figure 3 shows an infrared transmission spectrum of a film deposited in the absence of Hg backpressure (< 10^{-6} Torr). Instead of showing an absorption edge at 4 μm as expected for a film with a stoichiometric $Hg_{0.7}Cd_{0.3}Te$ composition, the transmission cuts on at 1.05 μm. This corresponds to a film with very low Hg content. X-ray diffraction measurements indicate the presence of free tellurium. EDAX measurements indicate its composition to be $Hg_{0.06}Cd_{0.3}Te$. By assuming the sticking coefficients of Cd and Te on a room temperature substrate to be unity, the sticking coefficient of Hg atoms will then be less than 0.1!

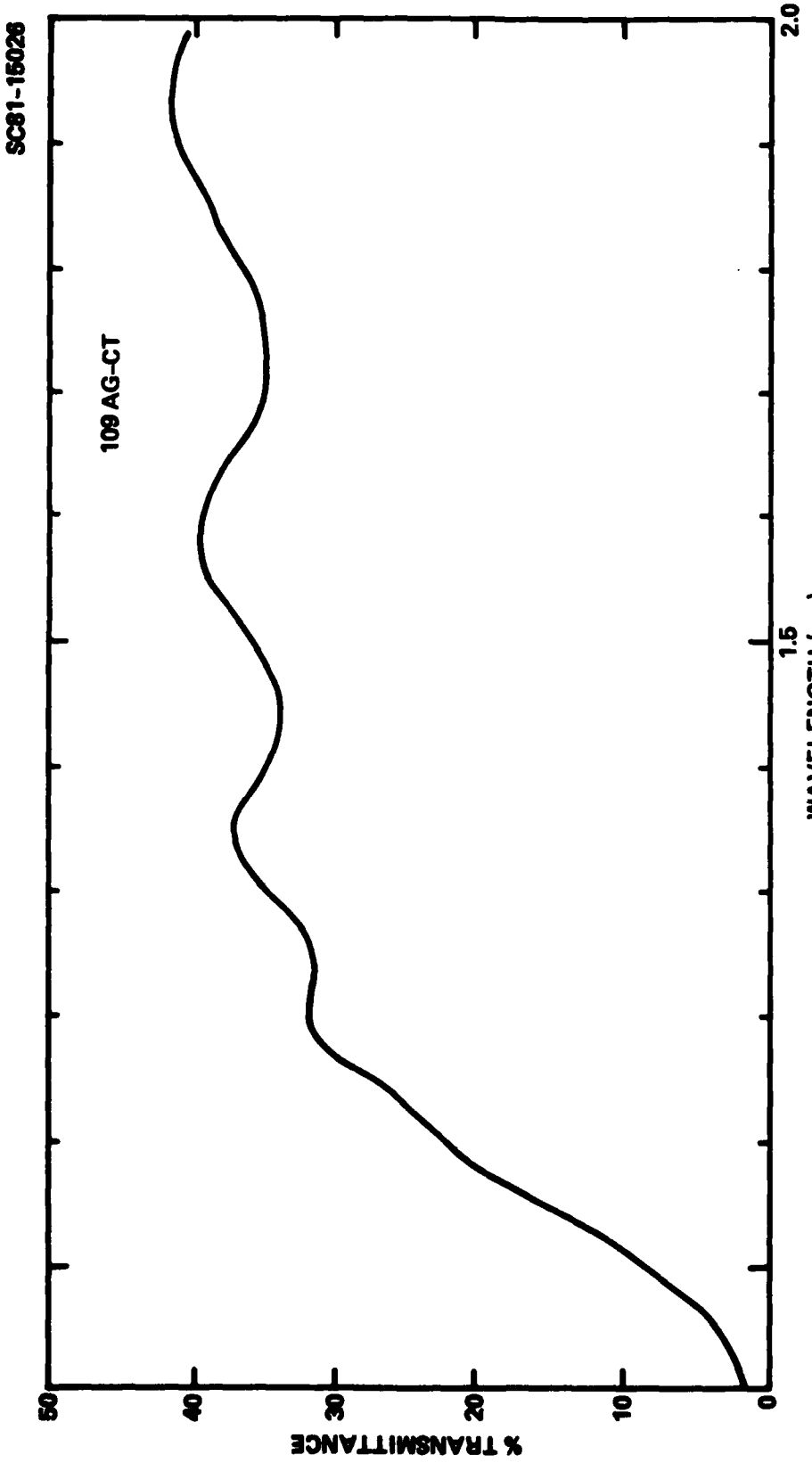

Fig. 3 Infrared transmission spectrum of a film deposited from a $Hg_{0.7}Cd_{0.3}Te$ target in Hg free vacuum.

Hg discrepancy can be compensated by carrying out the deposition in a Hg backpressure. Hg contents, f, expressed in terms of the fraction of stoichiometric Hg as in $Hg_{0.7}Cd_{0.3}Te$, is plotted as a function of P_{Hg} in Fig. 4. X-ray diffraction was used to determine if the film is stoichiometric. In a nonstoichiometric film, excess tellurium segregates into a second phase with characteristic diffraction peaks (see Fig. 5). In a stoichiometric HgCdTe film, tellurium diffractions are absent (see Fig. 6). The relationship is linear up to the saturation point. In other words, the dependence of Hg incorporation on P_{Hg} follows a first order kinetics. Under the conditions of this experiment, the saturation point is a Hg pressure of 8×10^{-5} Torr, above which stoichiometric $Hg_{0.7}Cd_{0.3}Te$ films can be formed. Within the pressure range studied here, the mean free path is too long for the gaseous interaction to be important. Therefore, any effect on incorporating Hg atoms into the film must be due to a gas-surface interaction. A deposition mechanism can be postulated in the following.

After the target material was irradiated with high power laser pulses, it evaporates congruently into atoms (Hg, Cd and Te) and a small amount of molecules (Te_2). When these species impinge onto the substrate surface, Cd and Te (Te_2) stick to the surface with nearly the same probability and recombine subsequently to form CdTe. The excess tellurium then reacts with Hg. Because of the weak HgTe bond, the probability for Hg to stay on the surface by HgTe formation is very low. The unreacted tellurium can be compensated by the background Hg. The amount of Hg backpressure required to react with all the free tellurium depends on the flux of the evaporants (i.e., growth rate) and substrate temperature. The amount of P_{Hg} which can be introduced into the vacuum system sets the upper limit of the deposition rate. In order to increase P_{Hg} thus elevating the growth temperature, one would have to heat up the entire vacuum chamber. We made a few attempts to increase P_{Hg} to higher than 10^{-3} Torr by heating up the Hg source and the entire vacuum chamber. We were able to elevate the substrate temperature to 140°C.

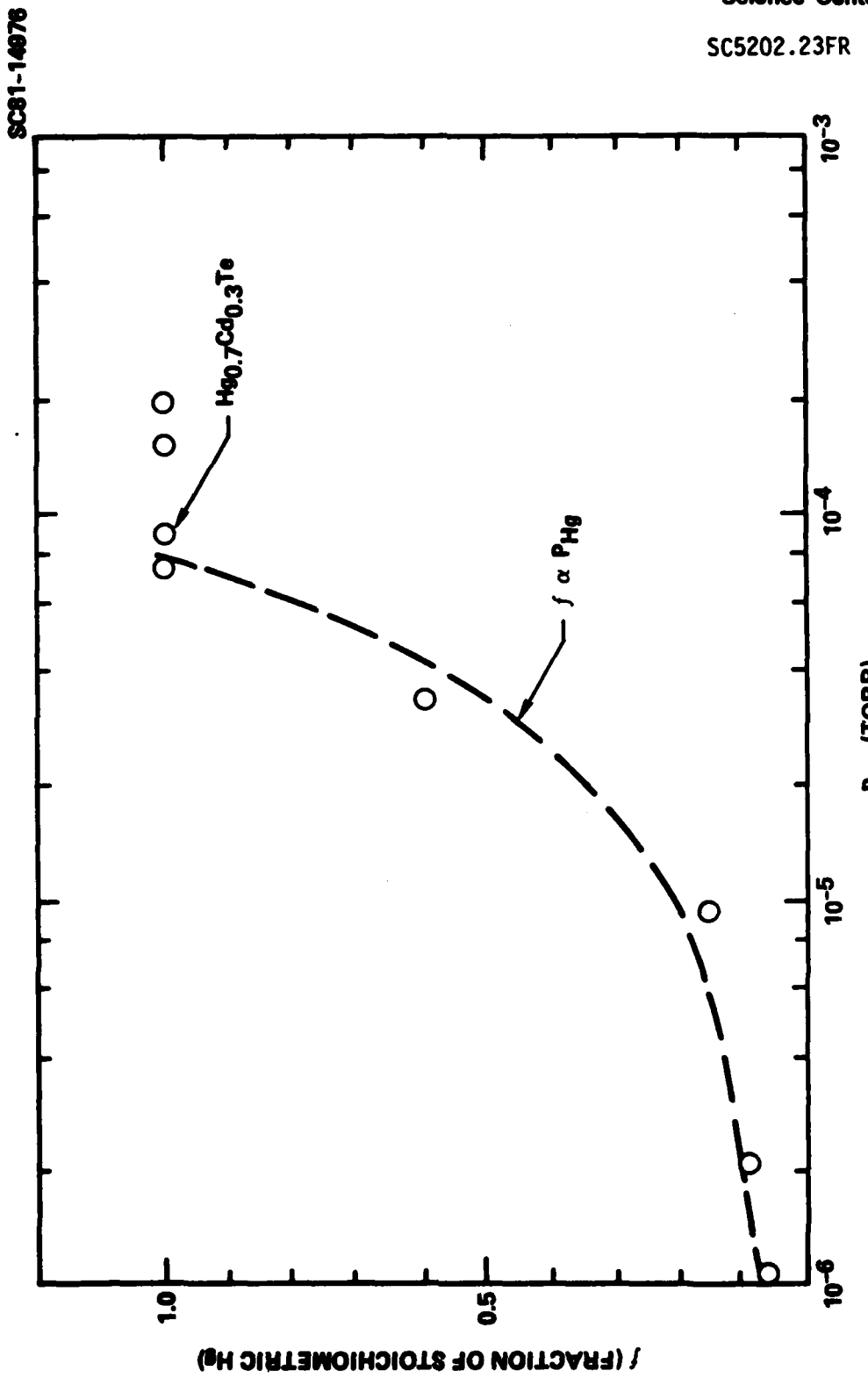

Fig. 4 Relationship between Hg content in film and Hg backpressure during deposition.

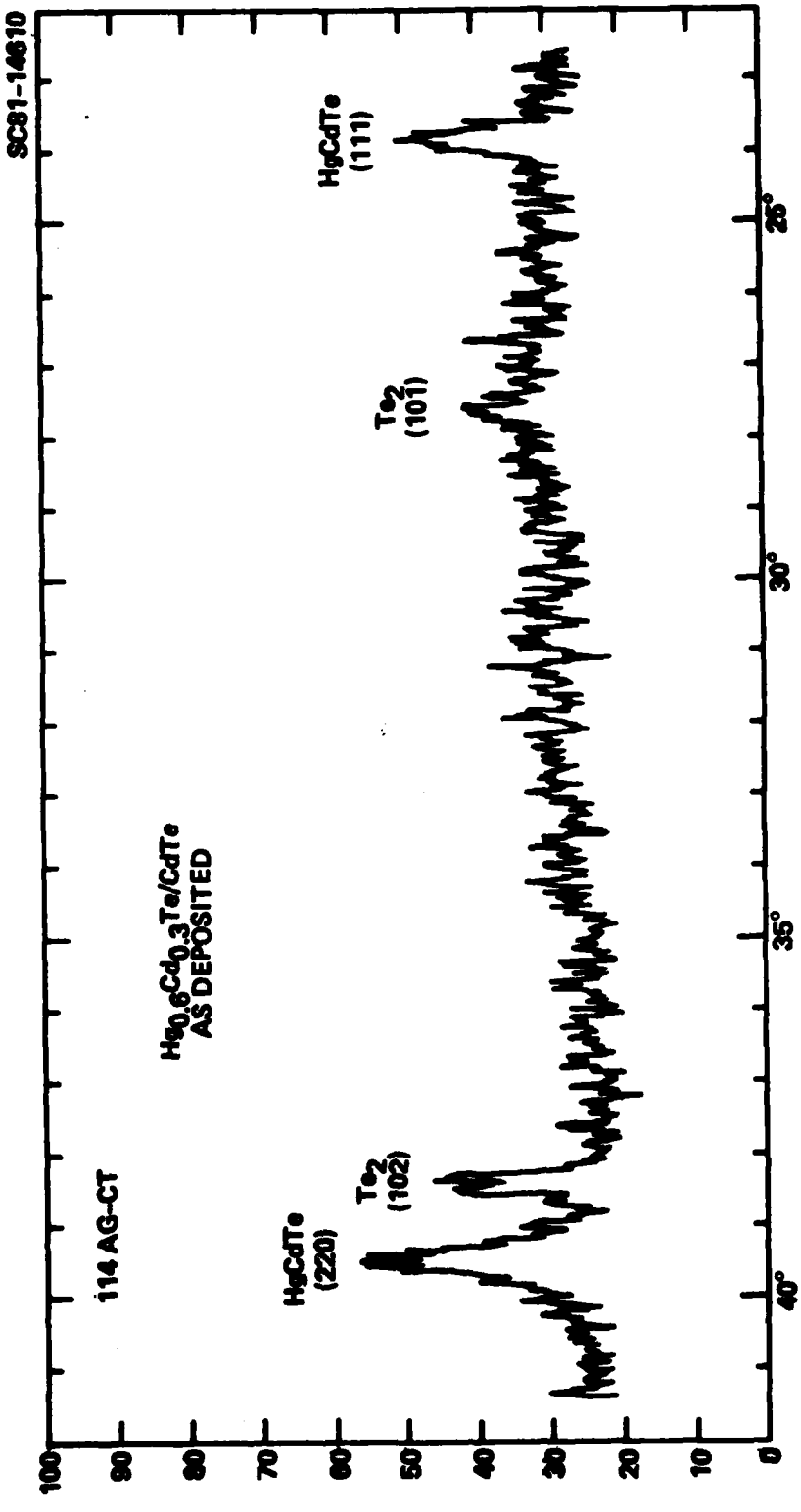

Fig. 5 X-ray diffraction spectrum of a nonstoichiometric HgCdTe film containing 10% free tellurium.

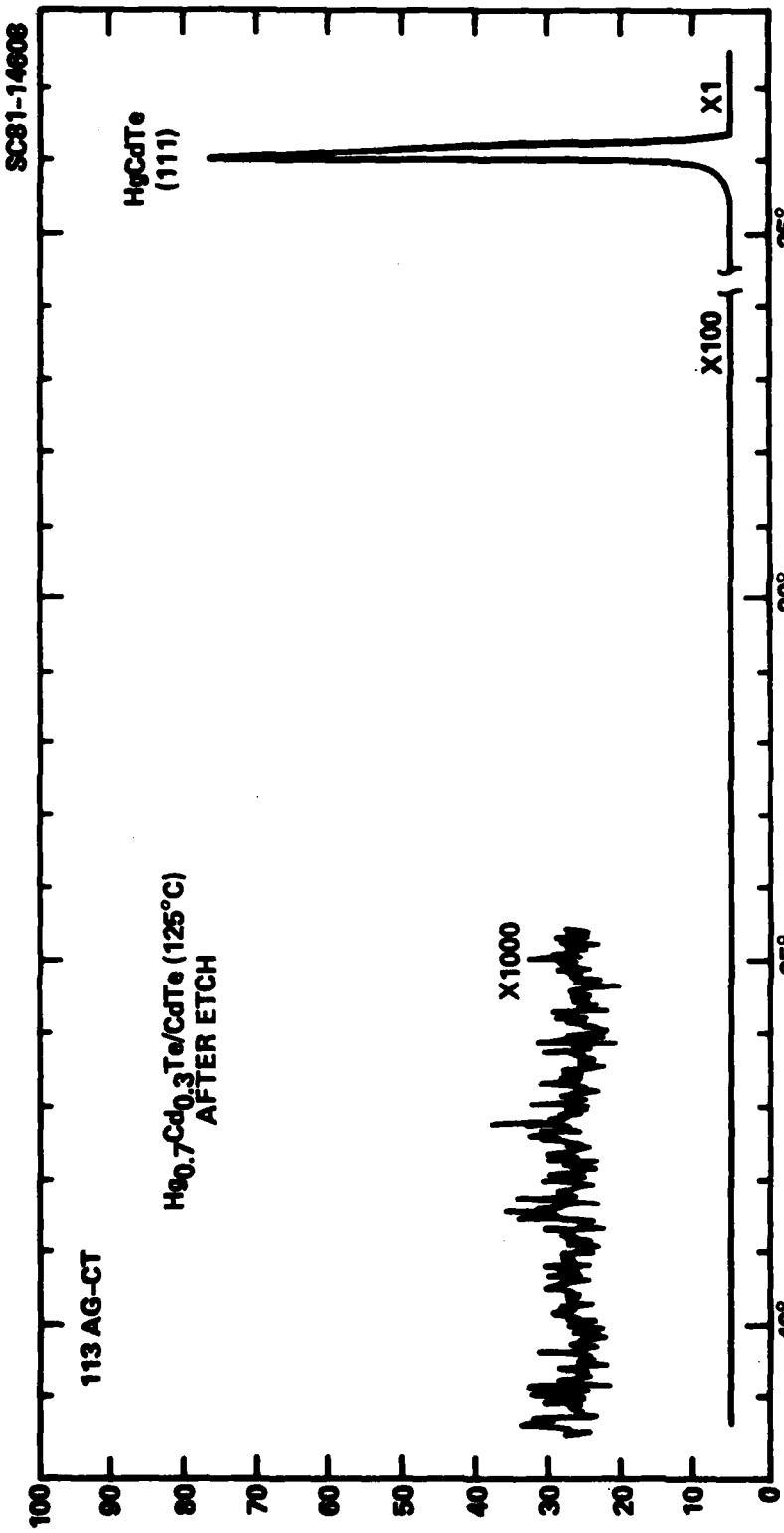

Fig. 6 X-ray diffraction spectrum of a stoichiometric $Hg_{0.7}Cd_{0.3}Te$ film.

However, the results were unsuccessful as films grown under this condition show poor electrical properties, presumably due to trapped impurities outgassed from the chamber wall.

At this point, it is appropriate to bring out the distinctive differences between laser assisted vaporization and thermal vaporization of CdTe, HgTe and their alloys. Interactions between high power laser pulses and CdTe (HgTe) are short but strong. The vaporization is different from that of a thermal evaporative process.

When high power laser pulses irradiate a source material, the radiation energy is absorbed by a shallow surface layer. Most of this energy is converted to heat. For poor thermal conductors such as HgTe and CdTe, heat redistribution by conduction is slow, therefore, the heating is localized. After the onset of a laser pulse, surface temperature increases rapidly to reach a peak value, followed by relaxing to nearly the original surface temperature before the arrival of the next laser pulse. Laser heating can generate very high peak temperature and short thermal cycles. Combination of these two effects causes materials to evaporate congruently and dissociatively.

HgTe evaporates noncongruently under equilibrium conditions. The mechanism was described as preferentially depleting Hg from the surface, while more Hg continuously diffused from the bulk to the surface to supplement the loss. In pulsed laser evaporation, Hg and Te evaporate simultaneously due to high peak temperatures and short thermal cycles. The thermal cycles are so short that the surface material is vaporized before Hg from the culk can outdiffuse. Therefore, congruent evaporation occurs. The same process has also been observed for $Hg_{1-x}Cd_xTe$ ($x = 0.2$ and $x = 0.3$) alloys. This is quite remarkable considering the vapor pressure of Cd and Te at 1000°C is orders of magnitude higher than that of Hg. The phenomenon is reminiscent of flash evaporation[10] but more flexible and precise.

High peak temperatures also induce dissociative evaporation, i.e., the source materials HgTe, CdTe and their alloys vaporize as atoms:

$HgTe \rightarrow Hg + Te$ congruent

$CdTe \rightarrow Cd + Te$

$Hg_{1-x}Cd_xTe \rightarrow (1-x)Hg + xCd + Te$. congruent

In contrast, conventional thermal evaporation produces atoms for the group II elements and molecules for the group IV elements, i.e.,

$Hg_{1-x}Cd_xTe \rightarrow (1-x)Hg + xCd + 1/2\ Te_2$ noncongruent

$HgTe \rightarrow Hg + 1/2\ Te_2$ noncongruent

$CdTe \rightarrow Cd + 1/2\ Te_2$.

The deposition processes are the reverse of these reactions. In LADA technique, it is atom-atom recombination. In conventional evaporative techniques, it is atom-molecule reaction. The generation of an atomic beam free of molecular and polymeric species has long been sought in many molecular beam epitaxy experiments. There is evidence showing that deposition by atomic beams results in films of higher quality. In molecular beam experiments, there have been attempts to produce atomic beams. Most notable approaches are the use of a two temperature cracking furnace, and the use of pyrolytic decomposition of low pressure metallo-organic compound such as AsH_3.[11] Only partial decomposition into atoms has been achieved, due to thermaldynamic limitation. In LADA, CdTe, HgTe and their alloys evaporate exclusively into atoms. Thus, it provides a simple and reliable way for making atomic beams. Recent work on the mass spectroscopic studies of thermal and laser-assisted evaporation of $As_{1-x}P_x$ alloy indicates 100% dissociation into atoms due to

pulsed laser irradiation.[12] It is believed that by proper choice of the laser, all semiconductors can be evaporated into atoms. Formation of a film of compound from atom-atom recombination presents some advantages. It does not require any activation energy to break the molecular bond of a reactant. In addition, the reaction is always exothermic. The amount of released energy is equal to the bond energy of the formed compound. The energy will be dissipated in the vicinity of the deposition site and provides localized heating to the as-grown film and enhances mobility of the surface atoms. A detailed study to compare the effects of laser evaporation vs thermal evaporation is underway.

3.1.1.2 Effects of Laser Power Density

Strong correlation exists between the laser power density for evaporation and the structural as well as electrical properties of the deposited films. Crystallographical qualities as well as surface morphology are dependent on laser power as determined from x-ray diffraction measurements. Figure 7 shows the surface morphology of three layers deposited under different power densities. Their growth conditions were otherwise identical. At 2×10^7 W/cm^2, the surface is very rough showing about 50% particle coverage with average size being 3 μm. The cross sectional view also shows trapped particles which are due to "spitting" from the source material. "Spitting" is a unique phenomenon associated with laser evaporation. It occurs when a subsurface layer is superheated by excess radiation before the surface itself is vaporized. Consequently, the superheated subsurface material explodes and ejects particles. "Spitting" phenomena at such low laser power densities was only found in the case of HgCdTe and HgTe. No spitting from CdTe was observed under the same laser power density. The low power density threshold for spitting is likely due to decomposition and boiling of mercury in the sublayer. This effect can be reduced by lowering the laser power level. At 5×10^6 W/cm^2 the average particle size is reduced to 1 μm and the surface coverage is considerably lower. At 5×10^5 W/cm^2, spitted particles become negligible. Crystallinity also improved with the

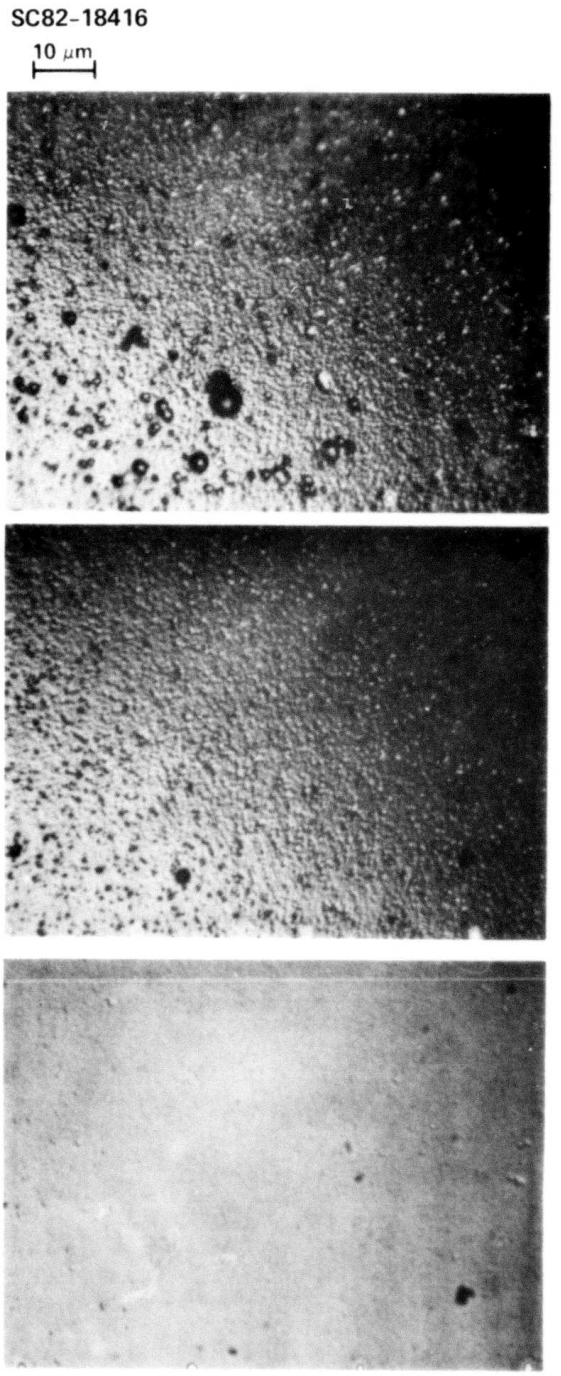

Fig. 7 Surface morphology of LADA HgCdTe layers grown under different laser power densities.

reduction of spitting. The width of <111> x-ray diffraction peak decreased from 12 min for 2×10^7 W/cm^2 power level to 3-4 min for 5×10^5 W/cm^2 power level, respectively. Electrical properties also improved accordingly. Results will be discussed in the next section.

3.1.1.3 Electrical Properties and their Dependence on Growth and Annealing Conditions

Electrical properties of LADA-grown films depend on many factors. Growth conditions (such as rate, substrate temperatures, Hg backpressure, laser power density, laser scan rate, impurity contaminations), as well as post growth annealing conditions (temperature, duration) can affect the quality of a film. Some of these parameters are interdependent. During the course of this program, it was impossible to establish separate empirical relationships between film quality and each individual parameter. Only some were identified and correlated.

Hall mobility and carrier concentration were measured by four-point Van der Pauw technique at 300K and 77K. Measurements were made from 4K to 300K for selected samples. Indium contacts were used for n-type samples and gold contacts were used for p-type samples. Post growth annealings (for p-type conversion) were carried out in sealed quartz ampoules with Hg back-pressure at 210°C and 410°C. Annealing time was 4 h.

During the early stage of this program, a laser power density of 5×10^6 W/cm^2 was used to evaporate $Hg_{0.7}Cd_{0.3}Te$. Films deposited on CdTe substrates at 130°C under this laser condition assume the morphology shown in Fig. 5(b). At 300K they are n-type with carrier concentration and mobility ranging from 3-5 $\times 10^{11}$/cm^4 and 700-1200 cm^2/V-s, respectively. At 77K, the films became highly resistive, i.e., low mobility, low carrier concentration, so that their electrical properties could not be measured. After annealing at 210°C, the 77K carrier concentration became 1-2 $\times 10^{17}$/cm^3 and mobility ranged from 3500-6500 cm^2/V-s. This behavior is similar to the MBE HgCdTe layers grown at 110°C by Faurie,[13] who attributed the low mobility of the as-grown

layers at 77K to scattering from microdefects formed due to the low growth temperature. In our case, the major cause is also due to structural defects. These defects were formed mainly by "spitting." For films grown under optimized laser power level to reduce spitting (Fig. 6(c)), their mobility and carrier concentration values at 77K were in the range of 4000-7000 $cm^2/V\text{-}s$ and $0.7\text{-}3 \times 10^{16}$ cm^{-3}, respectively. After 210°C annealing in a Hg overpressure, results were $1\text{-}1.8 \times 10^4$ $cm^2/V\text{-}s$ and $5\text{-}7 \times 10^{16}$ cm^{-3}, respectively.

Figure 8 shows the temperature dependence of carrier concentration and mobility of a $Hg_{0.66}Cd_{0.34}Te$ measured from 5K to 300K. The mobility increased from 3000 $cm^2/V\text{-}s$ at 300K to a peak value of 19,000 $cm^2/V\text{-}s$ at 34K and then leveled off slowly at 15,000 $cm^2/V\text{-}s$ at 5K. Carrier concentration at 300K was $7\text{-}5 \times 10^{16}$ cm^3. It decreased slowly with temperature and reached an asymptotic value of only 4.4×10^{16} cm^{-3}. Further annealing of this sample at 410°C for four hours reduced its carrier concentration to $1.2 \times 10^{16}/cm^3$ at 77K, but the film remained n-type and did not show any increase in the mobility. MIS capacitors were made by using a layer of native oxide with an overlayer of E-beam evaporated ZnS as insulator covered with 3 mm square metal dots. Very uniform MIS capacitance-voltage curves measured at 1 MHz frequency were obtained on all ten devices. Results are shown in Fig. 9. The data showed flat-band voltage at $V_{FB} = -4.5 \pm 0.1$ V, carrier concentration of $N_D = 7 \times 10^{15}/cm^3$ and a hysteresis of 0.2 V. All measurements were performed at 77K.

For as-grown layers with $Hg_{0.8}Cd_{0.2}Te$ composition, the 77K carrier concentration and mobility were $3 \times 10^{16}/cm^2$ and 24,000 $cm^2/V\text{-}s$ respectively. These values are very close to the MBE $Hg_{0.8}Cd_{0.2}Te$ layers grown at 120°C. Further improvements in the electrical properties can be expected by raising the growth temperature to near 200°C. Apparatus modifications are being undertaken to achieve this growth condition.

In order to fabricate photodiodes by ion implantation for IR detection, the base material needs to be p-type. The as-grown films were all

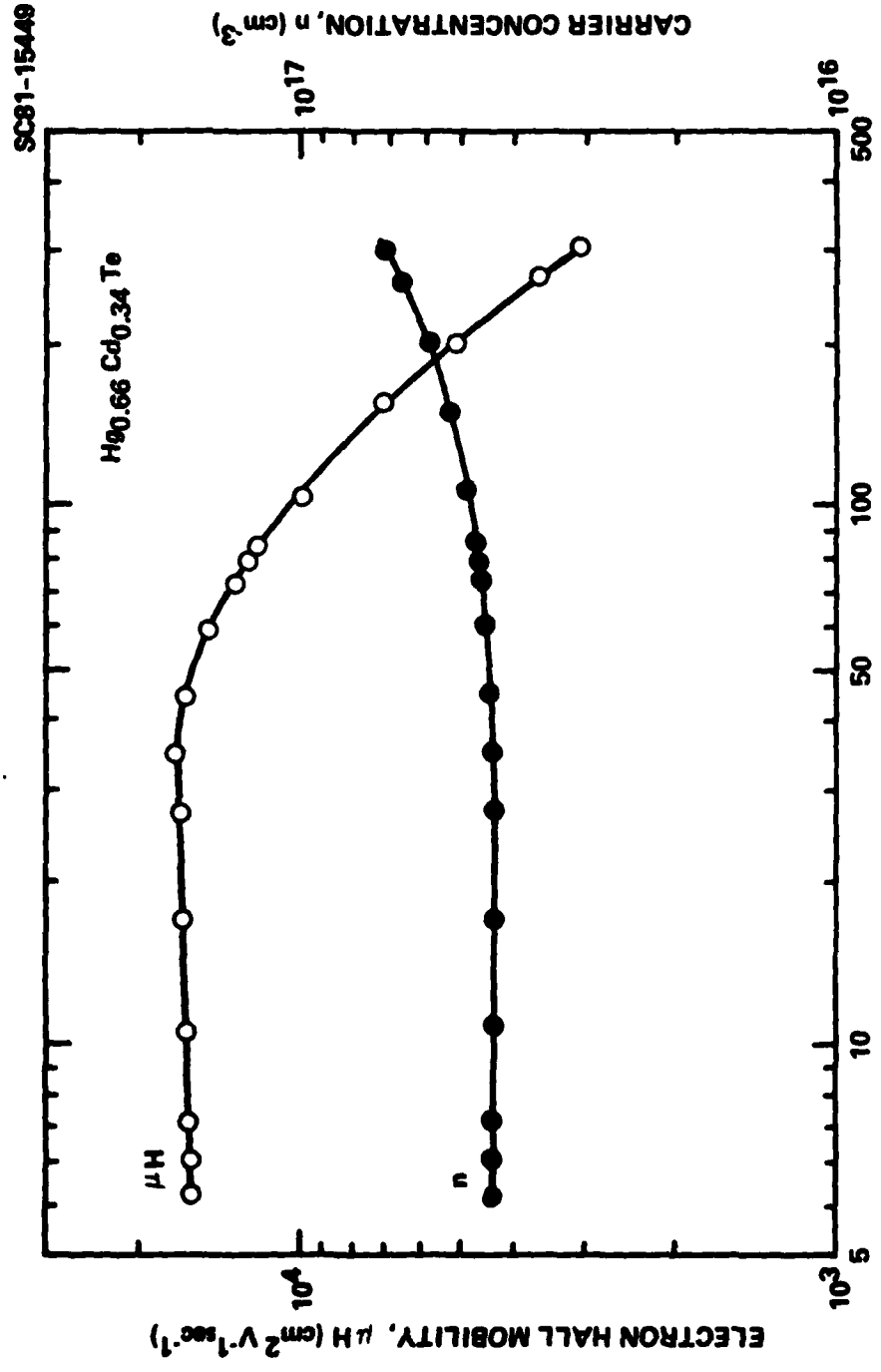

Fig. 8 Temperature dependence of mobility and carrier concentration.

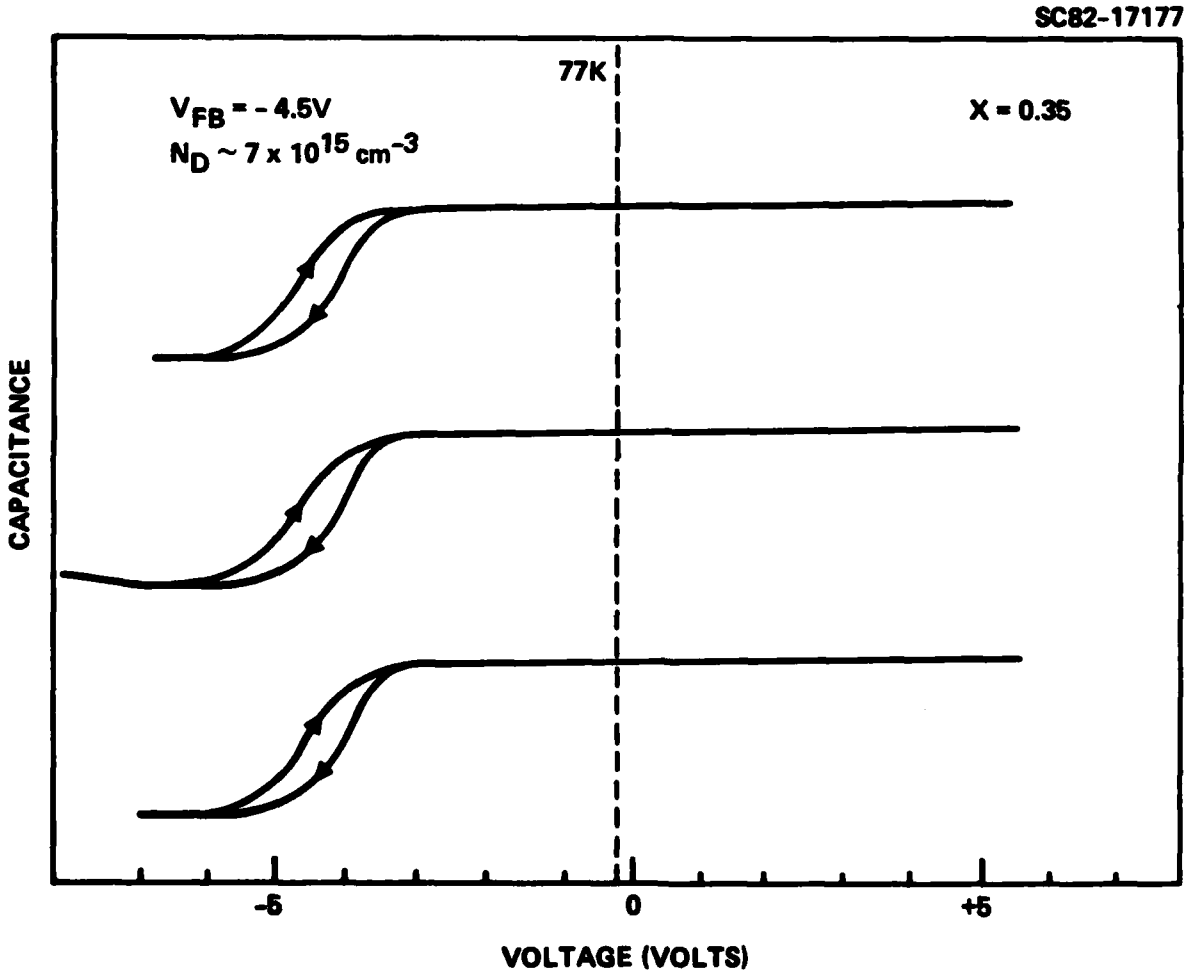

Fig. 9 C-V curves of LADA grown HgCdTe MIS devices.

n-type and remained n-type even after annealing under the p-type conversion condition (i.e., 410°C). One possibility for this persistence is the presence of high levels of donor impurities. Secondary ion mass spectroscopy (SIMS) was used for such analysis and identification.

Figure 10 shows the distribution profile of Hg, Cd and Te of an as-grown $Hg_{0.7}Cd_{0.3}Te$ film on CdTe. The compositional uniformity throughout the entire layer thickness is excellent and the transitional region at HgCdTe/CdTe interface is sharp due to low growth temperature.

Both the target $Hg_{0.7}Cd_{0.3}Te$ bulk crystal as well as the thin film were analyzed by SIMS for a number of impurities (i.e., Li, Na, Al, Si, Fe and B). In the bulk crystal, the contamination level of these impurities are too low to be detected. Therefore, the contamination must come from either the substrate or the deposition ambient. Figure 11 shows their distribution profiles. All impurity profiles show accumulation at the interface and near the surface with a minimum near the center of the film. Impurity distributions were also profiled for a thicker film (10 μm) as shown in Fig. 12. The same trend showed improved build-ups at the interface and near the surface. The most likely source is the impurities initially present on the substrate surface which is a result of the handling and exposure to the ambient. During the deposition, the film surface and film/substrate interface acted as getters, toward which the impurities diffused. Therefore, future LADA growth of HgCdTe should be carried out in UHV ambient for cleanliness. In addition, some in situ substrate cleaning procedures will be necessary and should include the growth of a buffer layer.

Among these impurities, Al and Si are known to be donors in HgCdTe. These impurities came from an unexpected source - the mirror mounted inside the vacuum chamber for deflecting the laser beam. Details of this discovery and its effect will be discussed in the following.

One difficulty in obtaining thick films by LADA technique involves the condensation of evaporants onto the vacuum chamber window through which the laser beam transmits. Condensation gradually reduces the transmission of

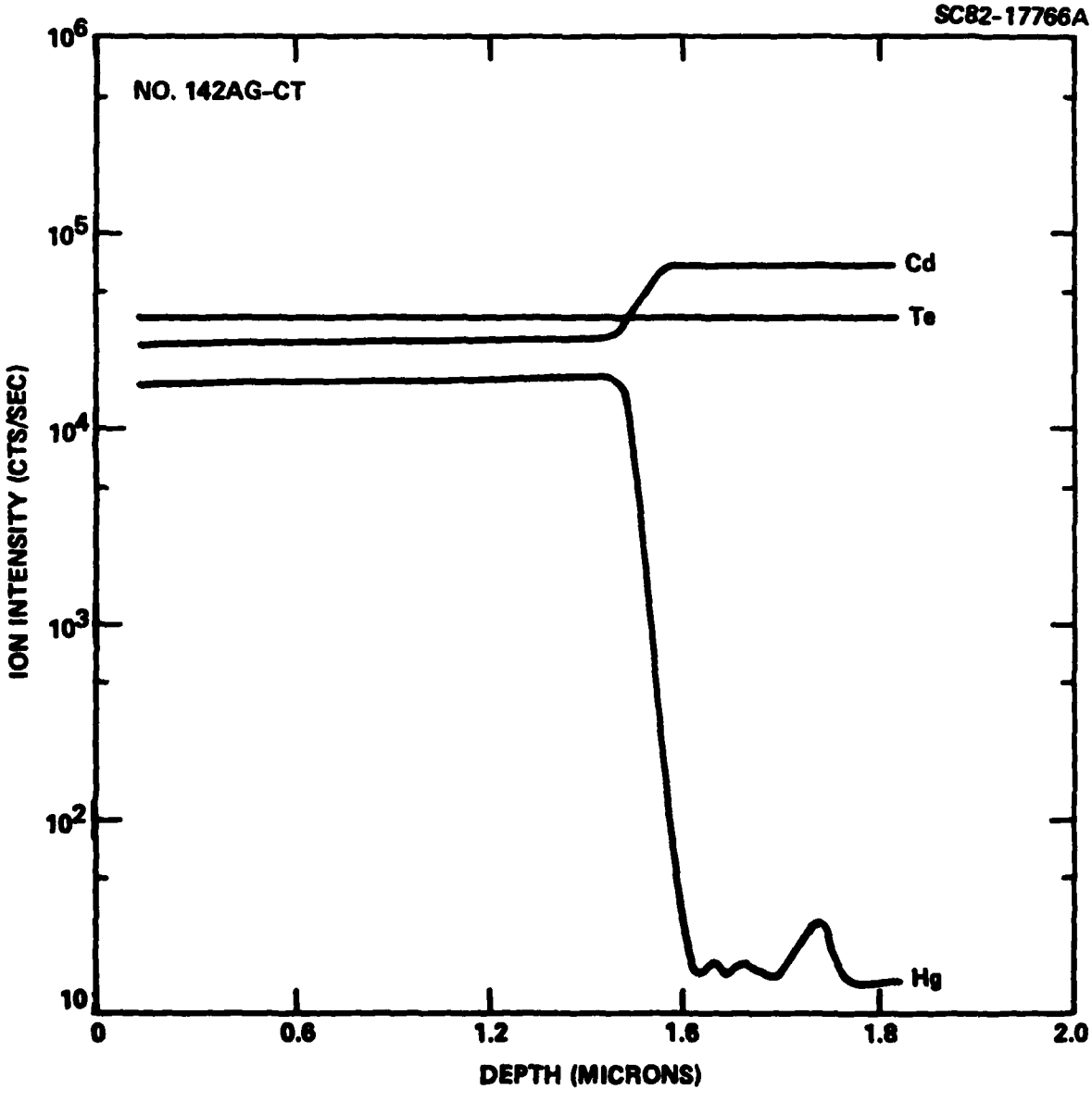

Fig. 10 Composition profile by SIMS.

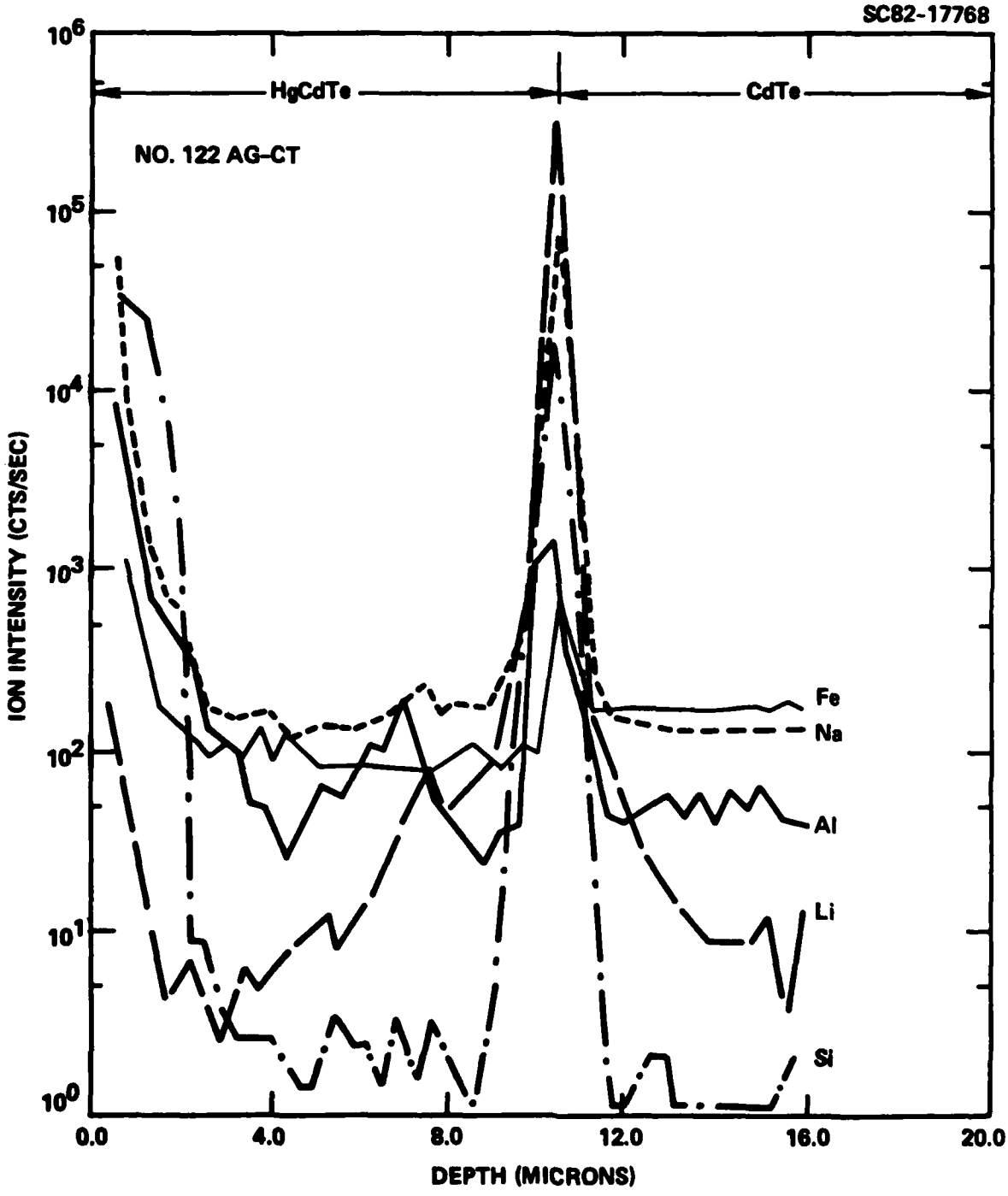

Fig. 11 Impurity profile of a thin sample.

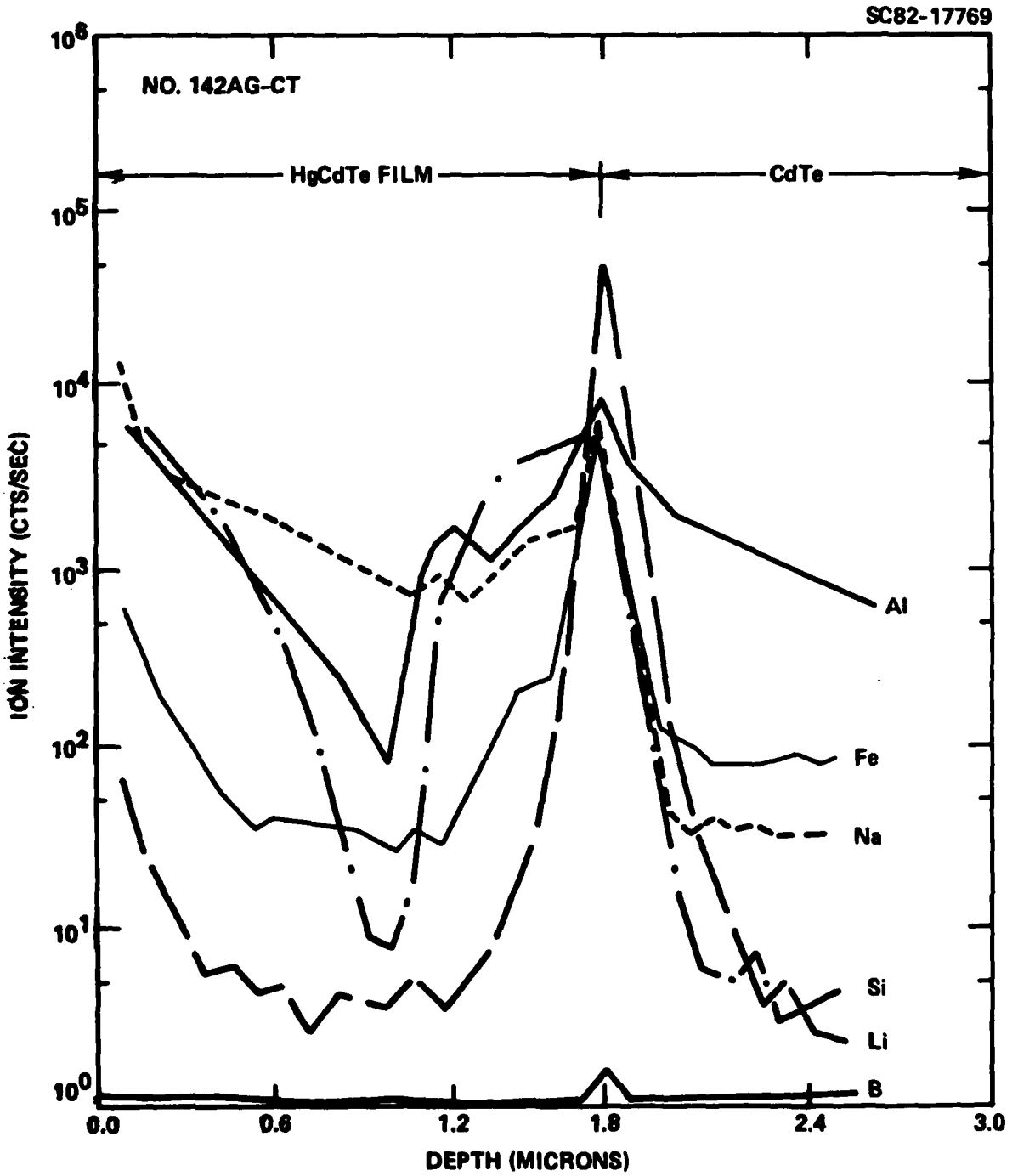

Fig. 12 Impurity profile of a thick sample.

the laser beam (i.e., the evaporation rate) until the window becomes completely opaque. Therefore, constant deposition rate cannot be maintained. To circumvent this problem, we first installed a light baffle to eliminate the line of sight between the target and the window. A first surface mirror, mounted on a tantalum wire heater, was installed inside the vacuum chamber to reflect the laser beam on the target. The mirror coating consisted of 2500Å aluminum covered with 2500Å SiO. Upon heating the mirror to 210°C or higher, the evaporants from the HgCdTe target did not stick to the mirror. Therefore, the mirror remained reflective at all times and thick films could be deposited.

The use of SiO/Al coated mirrors has one severe drawback. Under the experimental condition, laser radiation at the mirror surface was powerful enough to cause damage by melting and vaporizing the coating materials. Careful examination of the mirror surface before and after a few hours of laser irradiation revealed regions where SiO/Al coatings were completely removed. Both Al and Si (from SiO) could be incorporated into the HgCdTe film and resulted in the high Al and Si which led to the fact that these films could not be converted to p-type. After these findings, we replaced these mirrors. $Hg_{0.7}Cd_{0.3}Te$ films (No. 156) ~ 15 μm were grown under conditions similar to the previous runs. Annealing at 410°C for four hours was successful for p-type conversion. Mobility and carrier concentration at 77K were 125-140 $cm^2/V\text{-}s$ and 1-2 × $10^{16}/cm^3$ respectively.

Figure 13 shows the morphology and Laue x-ray diffraction pattern of an annealed p-type layer. It shows terracing with steps of a few hundred angstroms. Laue x-ray diffraction pattern is shown in the inset indicating a (111) oriented single crystal layer. We do not have any information on the effects of interfacial diffusion due to annealing.

Standard processing techniques were used to fabricate 6 mil × 6 mil square n^+/p implanted mesa photodiodes. The I-V curve and spectral response at 77K is shown in Fig. 14. The forward resistance is anomalously high. The spectral response peaks at 4 μm with (50%) cutoff at 50 μm. This cutoff

SC83-21458

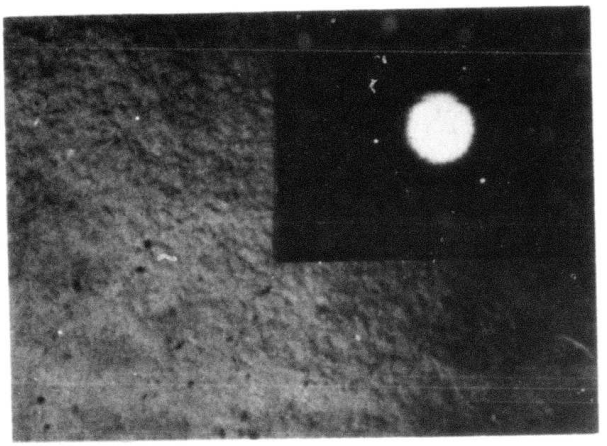

Fig. 13 Morphology of a $Hg_{0.7}Cd_{0.3}Te$ layer after being annealed to p-type.

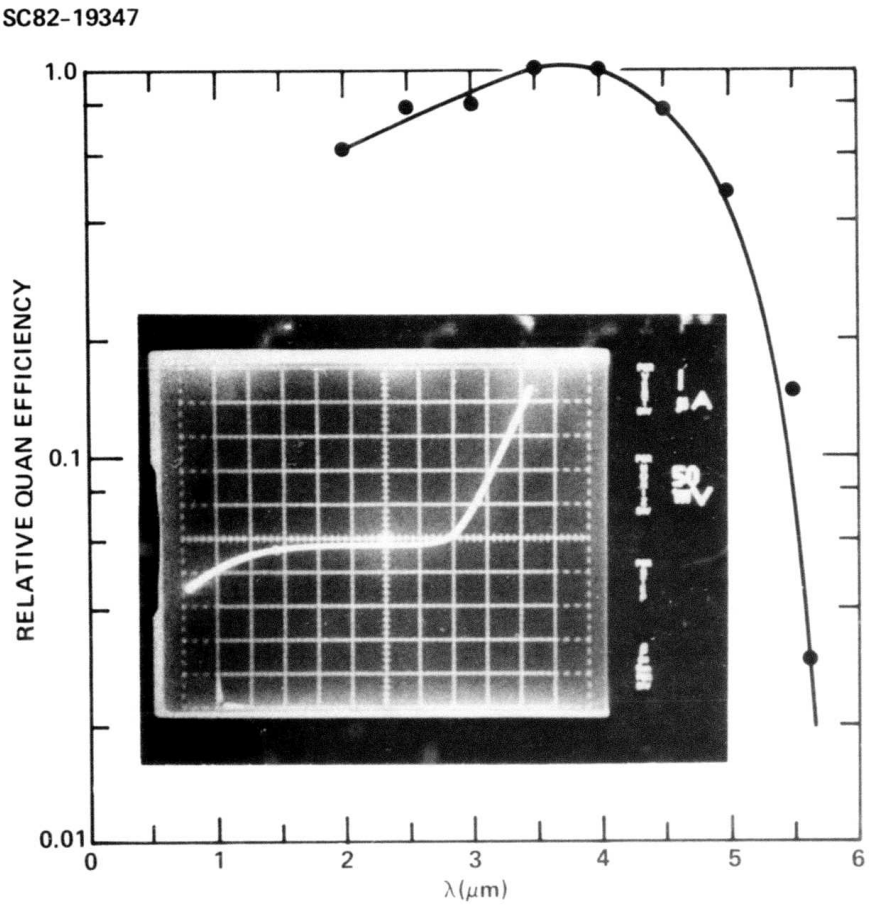

Fig. 14 I-V characteristic and spectral response at 77K for the first n^+/p photodiode fabricated on LADA $Hg_{0.7}Cd_{0.3}Te/CdTe$.

wavelength indicates a composition of x = 0.3 which is the same as the composition of the starting source material. This confirms the congruent evaporation nature of HgCdTe induced by pulsed laser heating.

3.1.1.4 Mixing of HgTe and CdTe by LADA

The experiments discussed above used a single evaporation target, namely, a piece of $Hg_{1-x}Cd_xTe$ bulk material. The source material must have high purity and must be stoichiometric. Requirements on crystallinity, electrical property, homogeneity and uniformity are not stringent, since the crystallographic and electrical properties of the film depend on the growth condition, and any nonuniformity and nonhomogeneity of the source material will not be carried over into the film due to continuous laser rastering and the layer to layer deposition process. However, the use of a single source does present one limit aside from economical consideration, that is, the limit of a fixed composition (x value) for a given target source. In order to grow thin alloy value with a certain composition, it must be preceded with the synthesis of a bulk material with the same composition.

We tried two approaches to circumvent the problem. In the first approach, we mixed HgTe and CdTe powders to a given proportion. The average size of these powder particles were about 1-2 μm. They were mixed thoroughly in a vibrating mill. The mixtures were then pressed into 0.5 in. diameter pellets under a pressure of 10 ton/cm^2 for two min. These pellets were used as source targets for HgCdTe deposition. Mass spectroscopic analysis of the evaporants during pulsed laser radiation were found to be the same as those from a bulk alloy. Indeed, the films deposited this way were found to have the desired composition which can be tailored to any value by choosing the composition of the mixture. Fig. 15 shows the comparison of infrared transmission spectra of two films, one by the use of a $Hg_{0.7}Cd_{0.3}Te$ bulk alloy and the other by the use of a pellet made from $(HgTe)_{0.7}/(CdTe)_{0.3}$ mixture. The cut-on wavelengths of the two are the same. Films made from powder mixtures are always inferior in quality, when comparing the films made from bulk

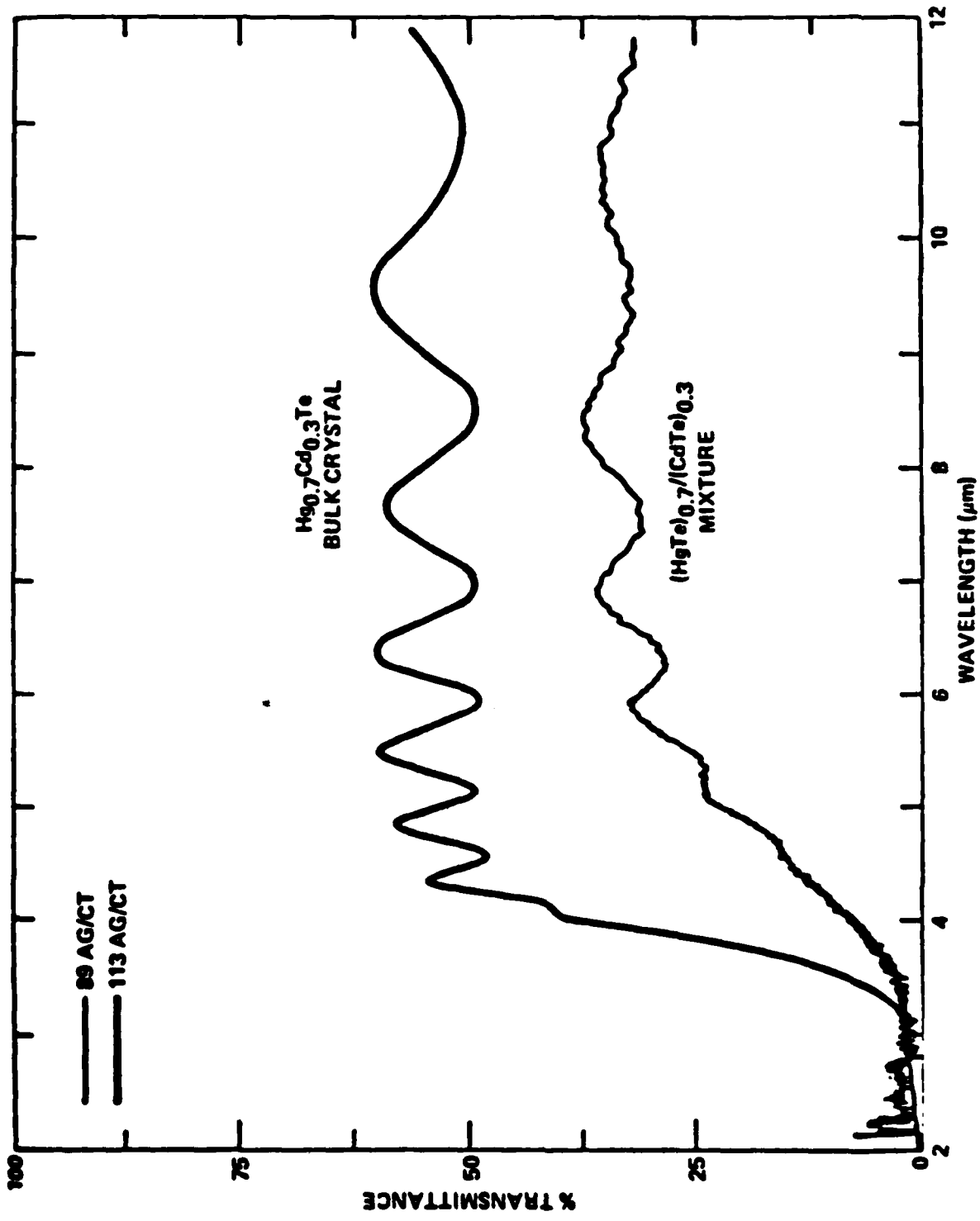

Fig. 15 IR transmission spectra of films deposited from $Hg_{0.7}Cd_{0.3}Te$ bulk crystal and $(HgTe)_{0.7}/(CdTe)_{0.3}$ mixture.

alloys. Their mobilities were about a factor of four lower and carrier concentration was about a factor of three higher. Their surfaces are always rougher. The poor qualities are attributed to a number of factors. First, powders have a very large surface area thus are more subjected to impurity contamination. Second, "air-pockets" exist between powder particles inside the pressed pellets. During pulsed laser irradiation, the "air-pocket" would heat up, expand and expel the particles before they were vaporized. This form of "spitting" could not be eliminated by lowering the laser power. We conclude that the use of powder mixture is not practical.

Another approach uses separate targets of bulk HgTe and CdTe which is inexpensive and easily available. These targets are placed side-by-side on rotatable holders. Laser beam is scanned repeatedly with a period τ over the two targets to cause alternate evaporation. In the case of short τ and high substrate temperature, interdiffusion between the arriving HgTe and CdTe can dominate over the layered formation. Complete alloying takes place. Let T_H and T_C be the time during which the laser beam dwells on HgTe and CdTe, respectively. Their ratio, which can be adjusted by the mirror scanner, determines the film composition. It can vary from x = 0 to x = 1.0. Figure 16 shows the optical transmission spectra of two films deposited with this approach. The ratio T_H/T_C was 1/3 for the first film and 3/1 for the second film. Their cut-on wavelengths vary accordingly. In both cases, scan period τ is 0.7 s. At a deposition rate of 2 μm/h, this period corresponds to the formation of less than one monolayer of HgTe and HgTe during each scan cycle. The substrate temperature was 120°C. Complete mixing is expected. This approach can be used to deposit $Hg_{1-x}CdTe$ of any composition; the composition can be changed abruptly at any time during the growth. Multilayer structures are variable compositions which opens up new possibilities for device structures. In fact, HgCdTe superlattice has been successfully demonstrated with this technique.[14]

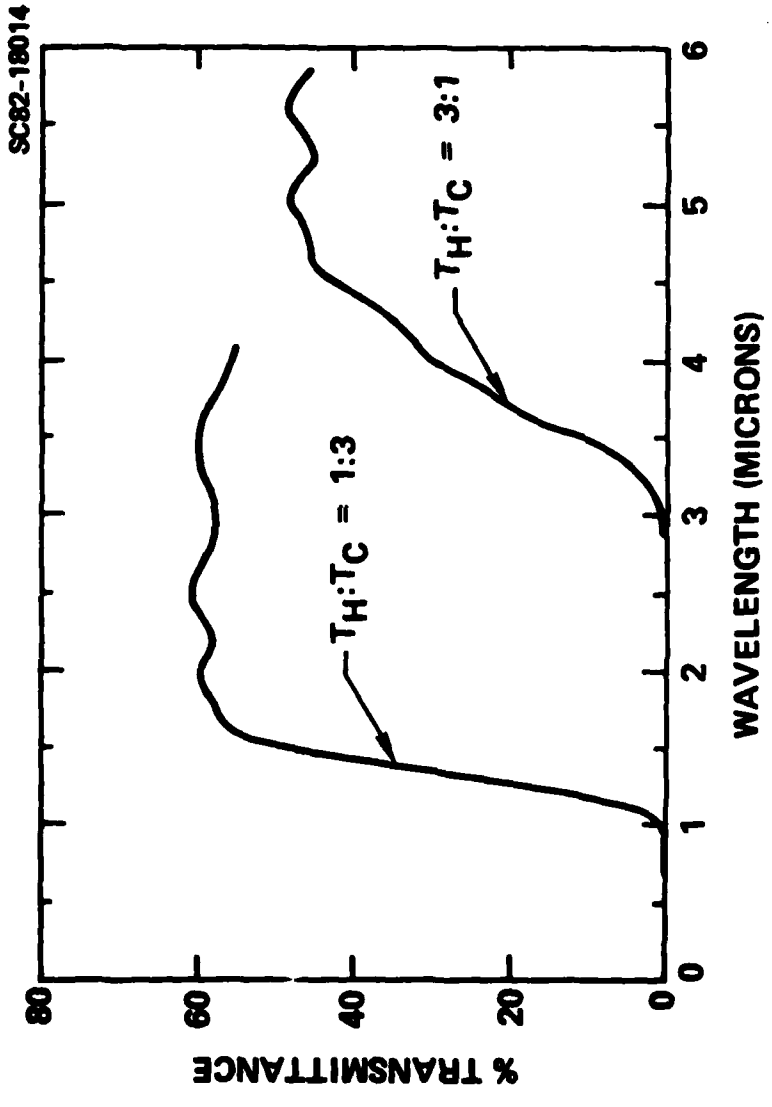

Fig. 16 IR transmission spectra of the two HgCdTe films deposited from LADA mixing of CdTe and HgTe.

3.2 CdTe/GaAs

One of ultimate goals of this work is to grow HgCdTe on a foreign substrate other than CdTe. We have tried to directly deposit HgCdTe on sapphire and Si[(111), (100)], but the films were all polycrystalline. Obviously, it will be best to first grow a high quality CdTe buffer layer which will then serve as a nucleation surface for the subsequent HgCdTe growth.

We have had great success using GaAs. Despite a large lattice mismatch (CdTe 6.482Å, GaAs 5.652Å), we obtained surprisingly high quality heteroepitaxial growth.

A total of more than ten films, 5 μm-14 μm, were grown on (100) GaAs substrates oriented to within ± 0.5°. The growth temperature recorded by a thermocouple placed in a hole on the back of the substrate holder was 350°C; the actual temperature of the substrate was lower. CdTe films grown on (100) GaAs exhibit (111) orientation. There are a few very small patches which show (100) CdTe growth. Figure 17 shows Nomarski micrographs of (111) and (100) CdTe grown on (100) GaAs substrates. The (100) CdTe films are very rough. They show streaking patterns parallel to the $\langle 1\bar{1}0\rangle$ direction of the substrate. They are most likely due to carbon residue on the surface. Resistivity at room temperature is 1.8×10^5 Ω-cm. The (111) CdTe films are extremely smooth with the only discernable feature being hexagonal aligned hillocks about two microns in size at a surface density of 10^4-10^5 cm^{-2}. These films are highly resistive with resistivity exceeding 10^6 Ω-cm (measurement limit). From the Laue x-ray diffraction pattern, which revealed x-ray backscattering from the CdTe film as well as the GaAs, we determined that one pair of the opposite sides of these hillocks are parallel to the $\langle 1\bar{1}0\rangle$ direction of the substrate (from selective etching).[15] LADA grown (111) CdTe on (111)A CdTe substrate also show a hexagonal hillock feature. Their opposite sides are parallel to the $[1\bar{1}0]$ axis of the $\langle 111\rangle$ substrate. From these relationships, we conclude that the $[1\bar{1}0]$ axis of the (111) CdTe films is parallel to the $[1\bar{1}0]$ axis of the (100) GaAs substrate. With this geometrical restraint, we overlap

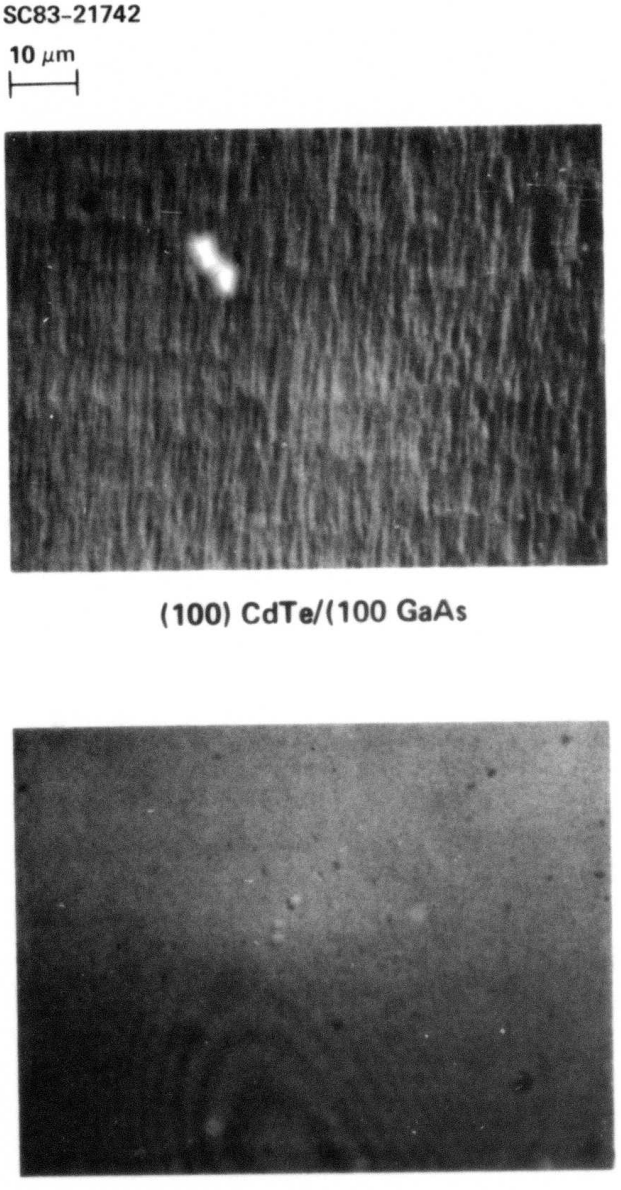

Fig. 17 Surface morphology of (100)CdTe/(100)GaAs (top) and (111)CdTe/(100)GaAs (bottom) heteroepitaxy.

(100) GaAs lattice with a (111) CdTe lattice as shown in Fig. 18. There appears to be a remarkable secondary epitaxial match corresponding to a super-cell containing atoms A, B, C, D, E. The lattice mismatch along the $\langle 1\bar{1}0\rangle$ and $\langle \bar{1}10\rangle$ directions are only 0.3% and 0.7% respectively! Whether this relationship is a geometrical coincidence or the actual happening can only be answered by more in situ analysis during the initial growth at the CdTe/GaAs interface.

UV reflectance spectra, Fig. 19, were taken from 200-420 nm for different CdTe samples. Both the (111) CdTe/(100) GaAs film and the chemically polished (111) CdTe bulk-grown wafer show practically identical spectra. The three peaks at 375 nm and 318 nm are characteristics of a zinc-blende structure.[16] This eliminates the possibility of a significant amount of wurtzite phase CdTe in the epitaxial films (characterized by reflection maxima at 360 nm and 305 nm). A photoluminescence spectrum taken at 77K is shown in Fig. 20. Good crystallinity is evidenced by the presence of the narrow band at 780 nm corresponding to bound exciton emissions.

The crystallinity was also examined by transmission electron microscopy (TEM), by T. Magee of Advanced Research and Application Corp. Standard jet thinning techniques were used to produce electron transparent regions in the CdTe layer. Horizontal or plan-view depth sections were obtained by chemically stripping a portion of the epitaxial layer and thinning the remainder of the specimen from the backside of the GaAs. The thickness removed by stripping was measured for each sample.

Figures 21(a) and 21(b) show representative bright field transmission electron micrographs obtained at various distances from the CdTe/GaAs interface. At distances < 2.3 μm from the interface, an extremely high concentration of defects is observed with dislocation densities typically > $10^{11}/cm^2$. At distances exceeding 2.3 μm, the dislocation line density is dramatically reduced, producing a zone of moderate dislocation density extending to the surface of the film. In Fig. 21(a) the electron micrograph obtained along the low angle wide depth section shows the existence of a clearly defined boundary

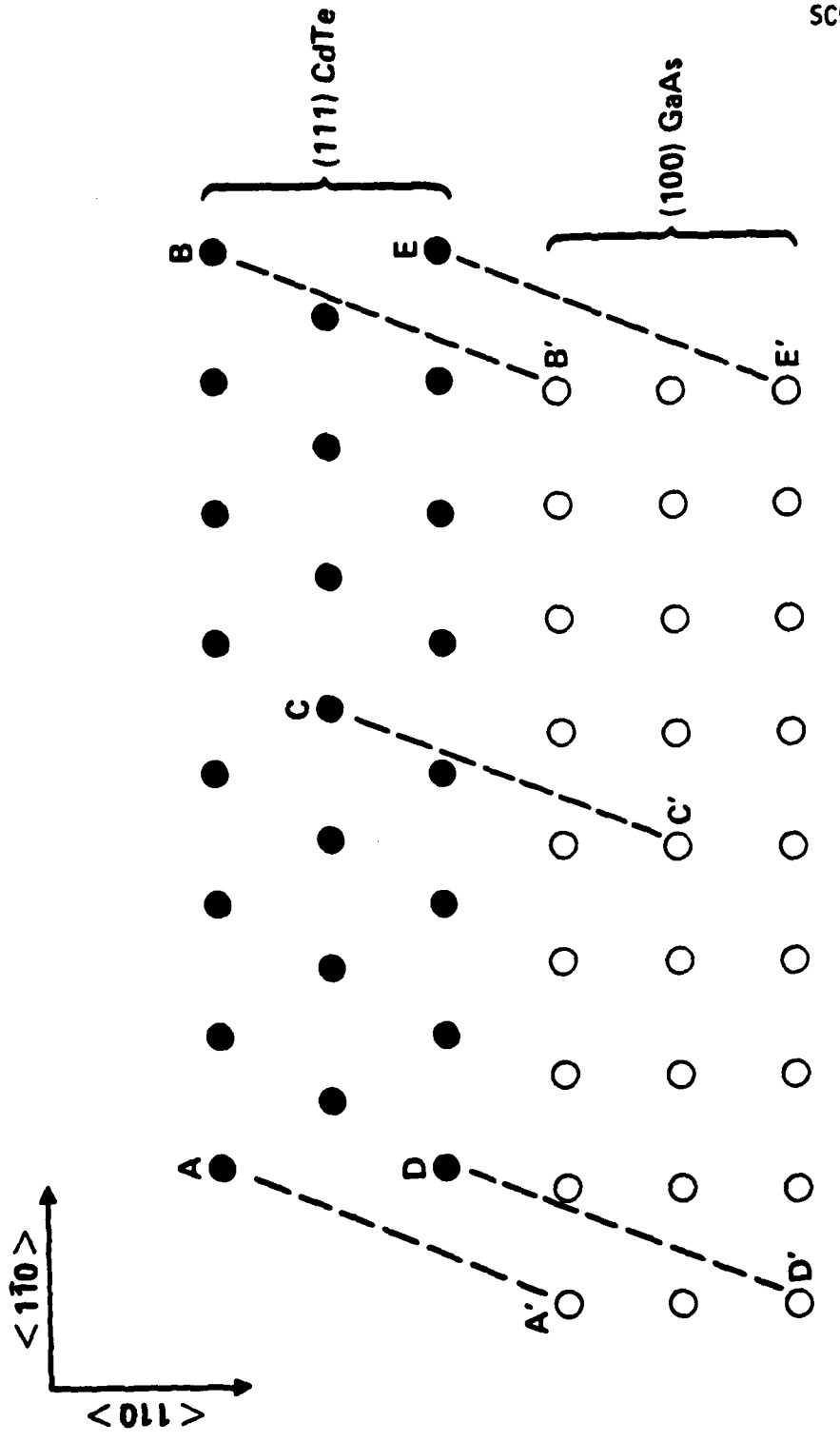

Fig. 18 Relative orientation and secondary epitaxial relationship for (111)CdTe/(100)GaAs heteroepitaxial structure.

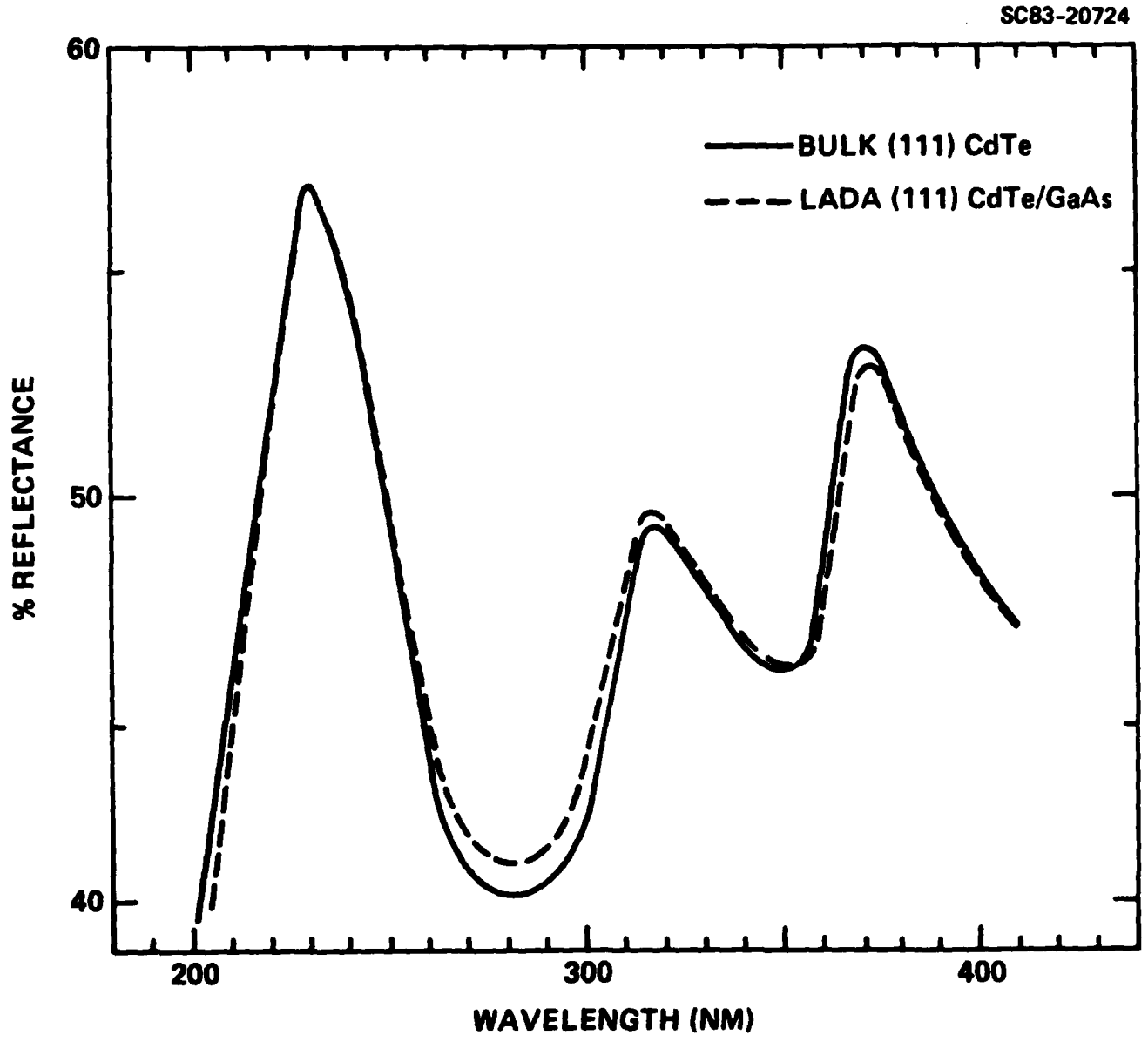

Fig. 19 UV reflectance spectra of a chemically polished bulk CdTe crystal and a LADA grown (111)CdTe/(100)GaAs layer.

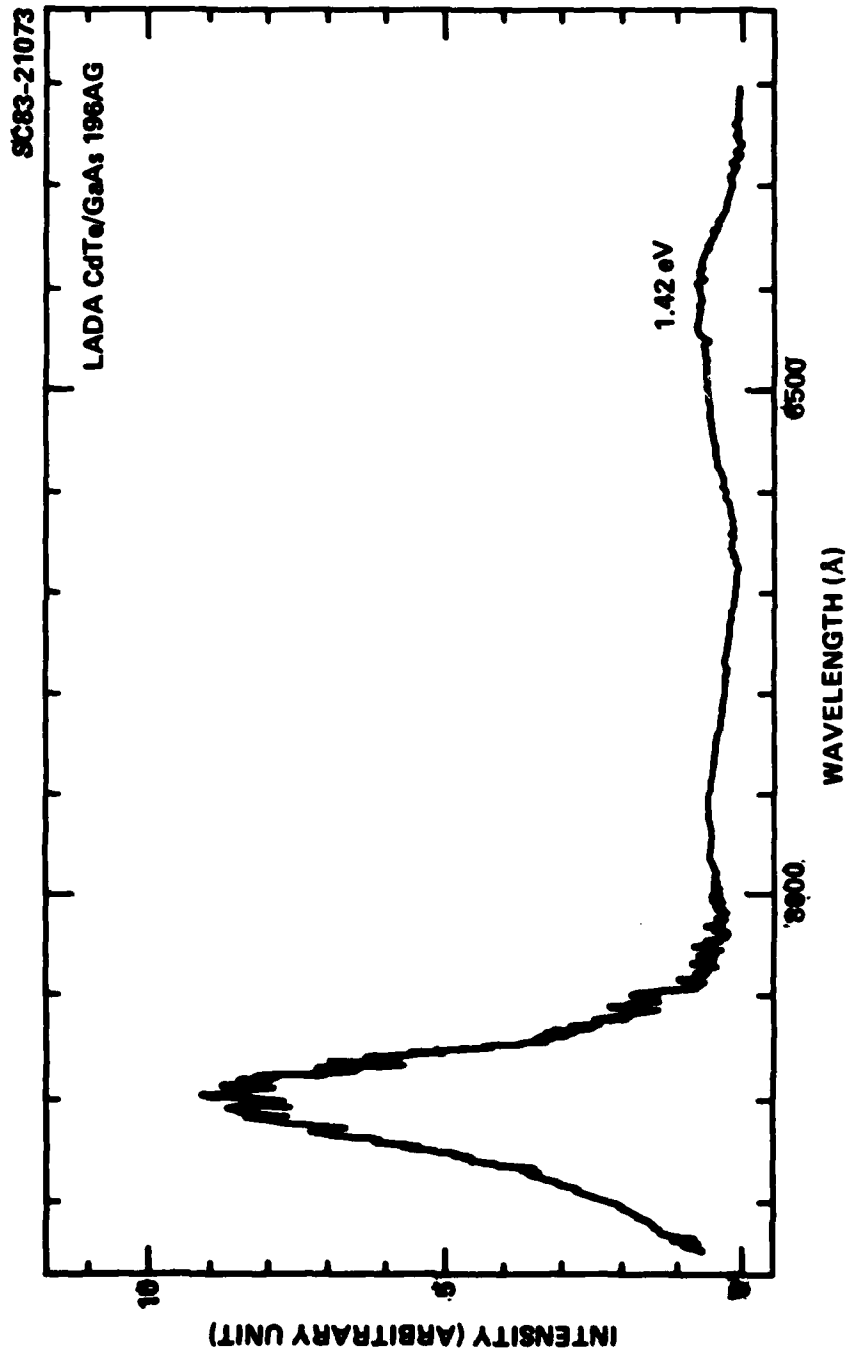

Fig. 20 Photoluminescence of (111)CdTe/(100)GaAs at 77K.

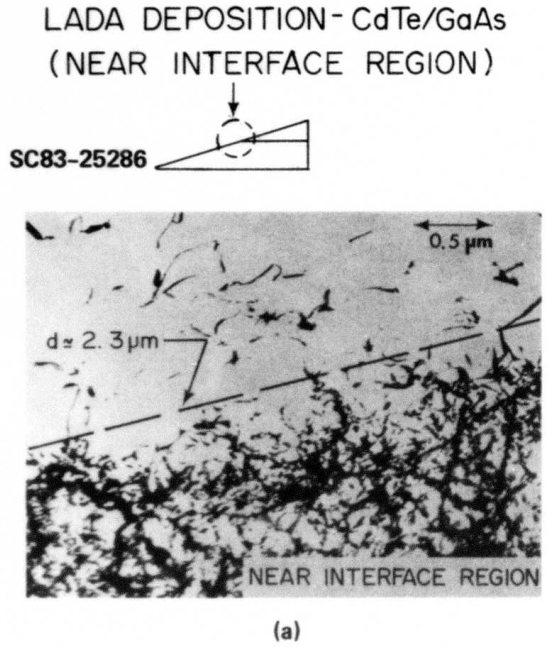

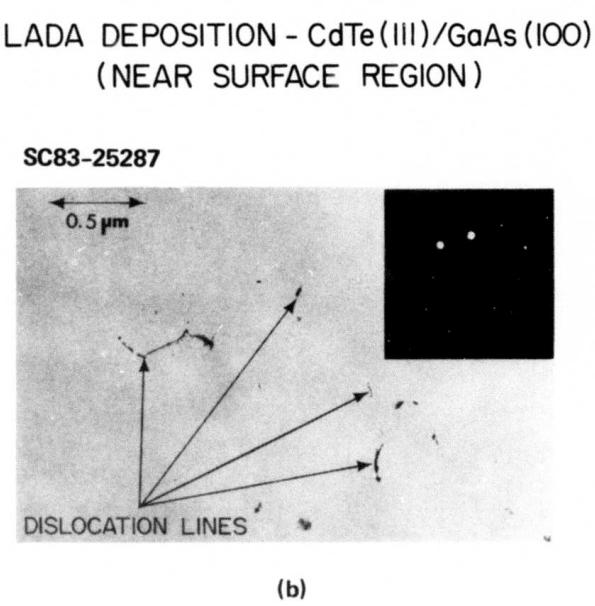

Fig. 21 (a) Bright field transmission electron micrograph obtained on sectioned CdTe/GaAs showing defect distribution in near-interface zone. (b) Bright field transmission electron micrograph obtained in near surface region of CdTe film on GaAs. Selected area electron diffraction pattern is shown inset.

between the two regions. Surprisingly, the reduction in defect density occurs over a relatively short distance, suggesting that misfit stress between the GaAs and CdTe is effectively accommodated over a distance of < 2.3 μm. This result may possibly be related to the relatively low deposition rate used in these experiments, thereby permitting the formation of complex nesting and dislocation line interactions which would then limit the forward propagation of threading dislocation and planar misfit networks. The large misfit between the two materials would result in effective "bending" of threading dislocation lines within the near-interface zone,[9] but would not necessarily limit the formation of planar misfit dislocations in the film.

Within the interior and near-surface regions of the CdTe film (Fig. 21(b)), the dislocation line density was observed as > $10^5/cm^2$. No evidence of complex nesting and dislocation line interactions was detected within near-surface regions of any of the films examined. In all cases, selected area electron diffraction patterns showed a (111) orientation within regions above the interfacial region.

The complicated nature of structure at the CdTe/GaAs interface will require extensive investigation. Additional experiments are underway to investigate the nucleation and growth processes for CdTe/GaAs.

We have tried an all LADA growth of a HgCdTe/CdTe/GaAs structure. After CdTe growth on GaAs substrate at 350°C, the substrate was cooled down to 100°C and the chamber was filled with 10^{-4} Torr of Hg backpressure. The growth rate for $Hg_{0.7}Cd_{0.3}Te$ was 2 μm/h. The layers were single crystalline as determined by Laue x-ray diffraction. Electrical property of this film was very poor with 77K carrier concentration (n-type) and mobility of 2×10^{15} cm^{-3} and 135 $cm^2/V\text{-}s$, respectively. The cause of such poor electrical properties is unknown. (111) CdTe/(100) GaAs heterostructure was also used for the growth of HgTe/CdTe superlattice. The results have been reported recently.[14]

3.3 ZnO

3.3.1 Evaporation of ZnO with CO_2 Laser Pulses

ZnO source materials were either sintered pellets or cold pressed pellet from high purity ZnO powders.

It was observed that powder size, packing density as well as the incident laser density and the beam scan rate all contributed to the evaporation rate as well as to the phenomenon of spitting of particulate material.

The absorption at 10.6 μm by ZnO powder particles will determine the local temperature of the pellet surface, hence the evaporation rate. The absorption is expected to be weak, since the restrahlen absorption band for ZnO occurs at 26 μm, with absorption peak width f about 10 μm (Fig. 22). In fact, a rough estimate of the absorptivity at 10.6 μm obtained from the ratio of forward and backscattered intensities to the incident laser power, gave values of about 20 cm^{-1}. The low thermal conductivity of the powder ZnO (5.8×10^{-6} cal/cm K s) causes the heat to be retained in the surface region. The spot, where the laser beam is focused, is heated to temperatures ~ 1000°C, as judged by radiometry. The intense heating probably causes the ZnO to decompose and to evaporate congruently. The calculated vapor pressure of Zn over ZnO and over Zn is shown in Fig. 23. Working back from the evaporation rate, as measured by the loss of pellet weight with time and calculating the vapor pressure of zinc, the temperature of a 100 μm diameter area, the spot size of focused CO_2 laser beam is found to be 900-1200°C, in qualitative agreement with visual observations. The fact that ZnO pellet retains its white color does not show Zn enrichment at the surface, indicating congruent evaporation. Congruent evaporation is achieved even under thermal decomposition of ZnO because of a relatively high vapor pressure of Zn for temperatures > 800°C.

The evaporant flux was analyzed by means of a residual gas analyzer. During laser evaporation, oxygen and zinc isotope signals dominated the RGA spectrum. ZnO signal at 81 amu was comparatively weak, about 1/100-1/1000 of Zn signal.

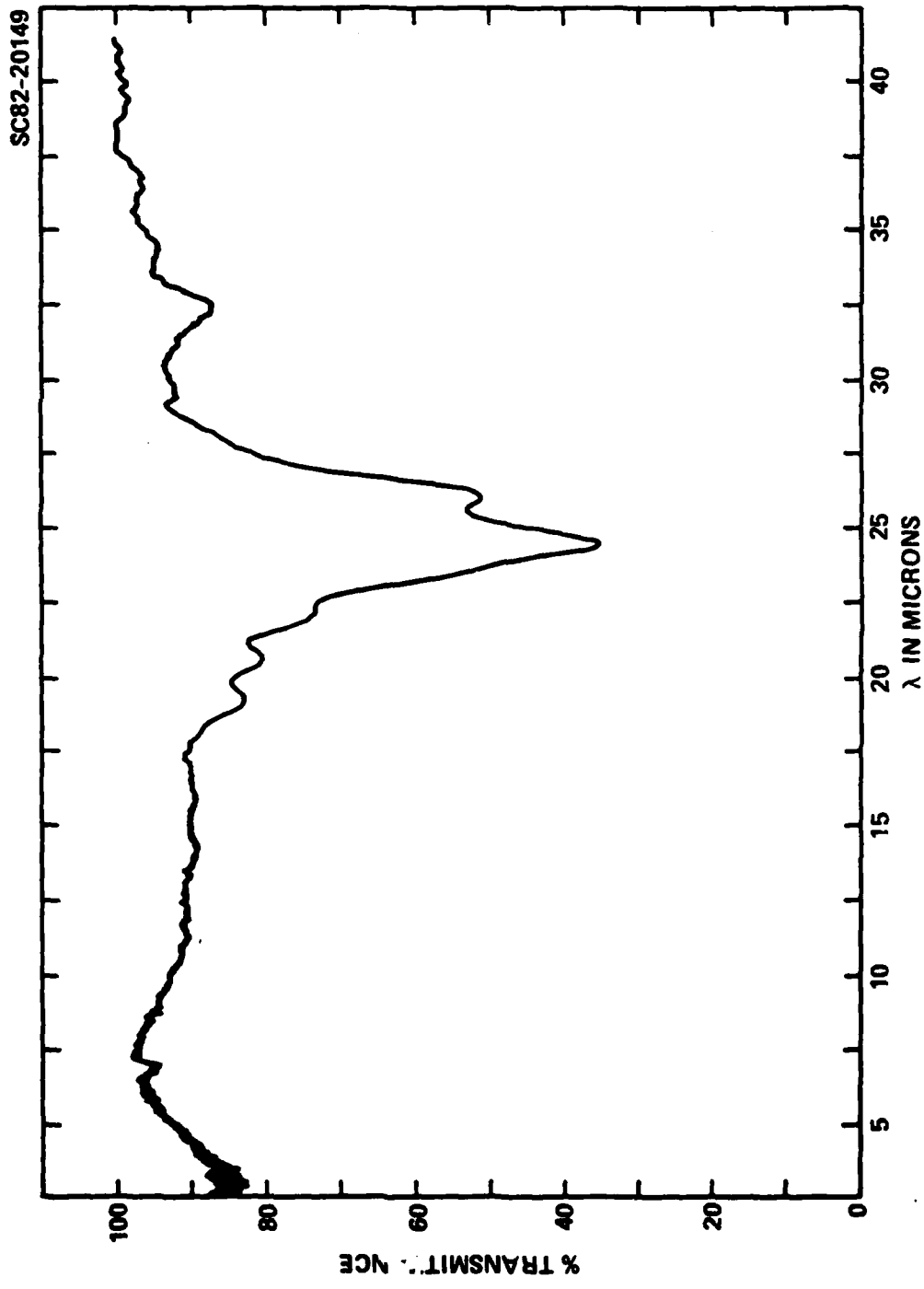

Fig. 22 IR transmission of a ZnO film.

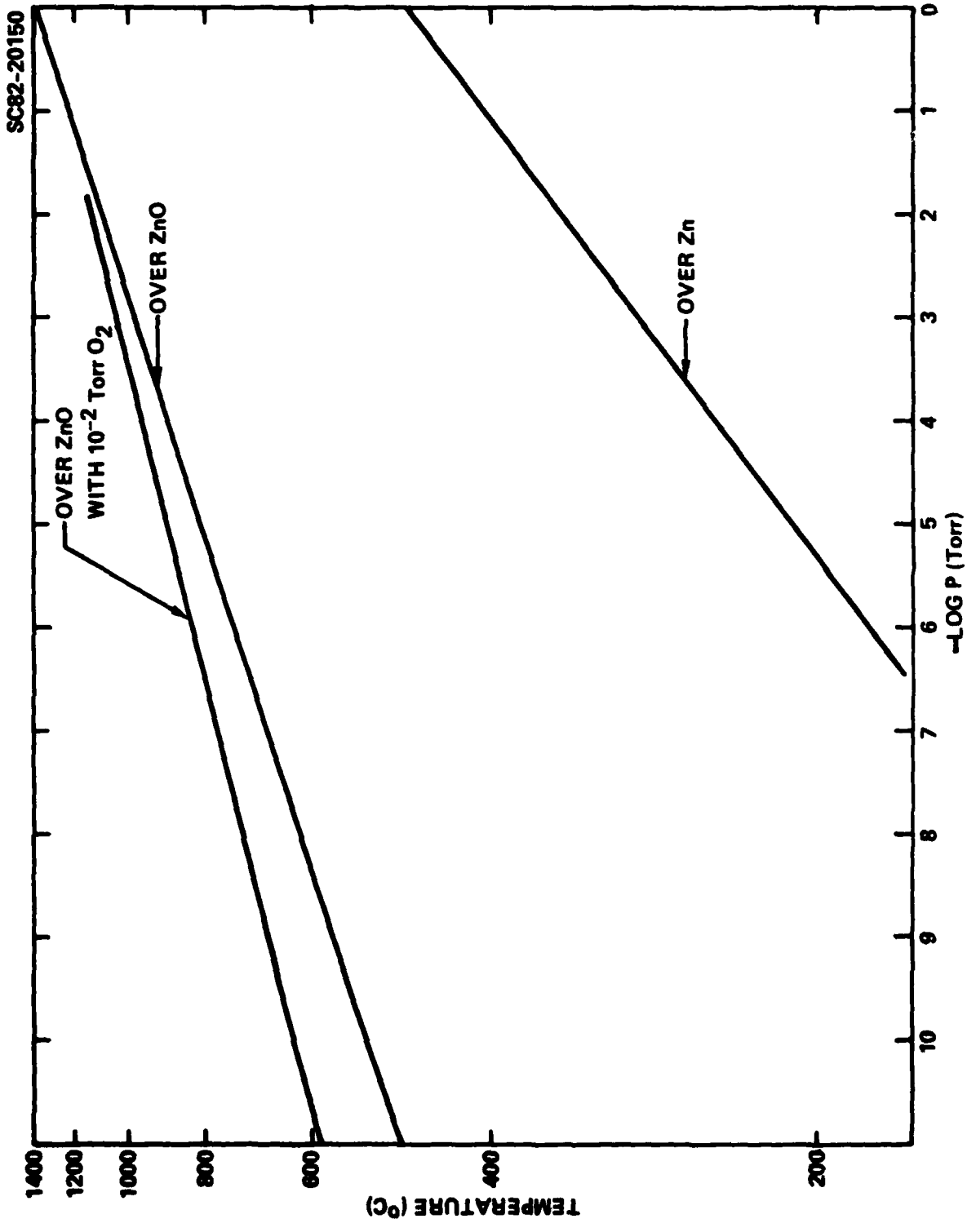

Fig. 23 Vapor pressure of Zn over ZnO and over Zn.

Zn and ZnO signals were observed to persist up to 1/4 h, following the turning off of the laser or when a shutter was interposed between RGA and ZnO source. The ZnO signal increased in magnitude when the cold trap was allowed to warm up releasing such oxidizing species as H_2O, CO, CO_2, O_2. These effects can be explained by assuming re-evaporation and oxidation of Zn deposited on and around RGA filament. The above observations suggest that ZnO molecular species do not exist in vapor phase, and laser evaporation of ZnO target produces Zn and O_2.

In another set of experiments, the ionization of the evaporant flux was measured. The experimental setup is shown in Fig. 24. Two large area electrodes flanked the pellet and were 2 cm apart and biased with respect to each other up to 250 Vdc. This bias was enough to deflect singly ionized species during their transit, even at high speeds of 10^5 cm/s, corresponding to energies in eV range. Such high energies have been observed in laser evaporation of metals. The current sensitivity of the electrometer was 10^{-13} A. No current was detected during laser evaporation at any power level of laser beam. This puts an upper limit on the number of ionized species in the evaporant flux of 1 part in 10^{14}. The conclusion is that evaporated species are not ionized, as would be expected from particle energies at thermal evaporation temperatures. The above fact indicates that biasing the substrate during evaporation will not effect the velocity of the impinging species in the direction normal to the substrate.

3.3.2 Deposition of ZnO

Our experiments indicate that the deposition of ZnO on the substrates proceeds by reactive evaporation of Zn with residual oxidizing gases in the vacuum environment. The oxidation of Zn proceeds rapidly due to exothermic nature of the reaction

$$Zn + \frac{1}{2} O_2 \rightarrow ZnO$$

SC82-20151

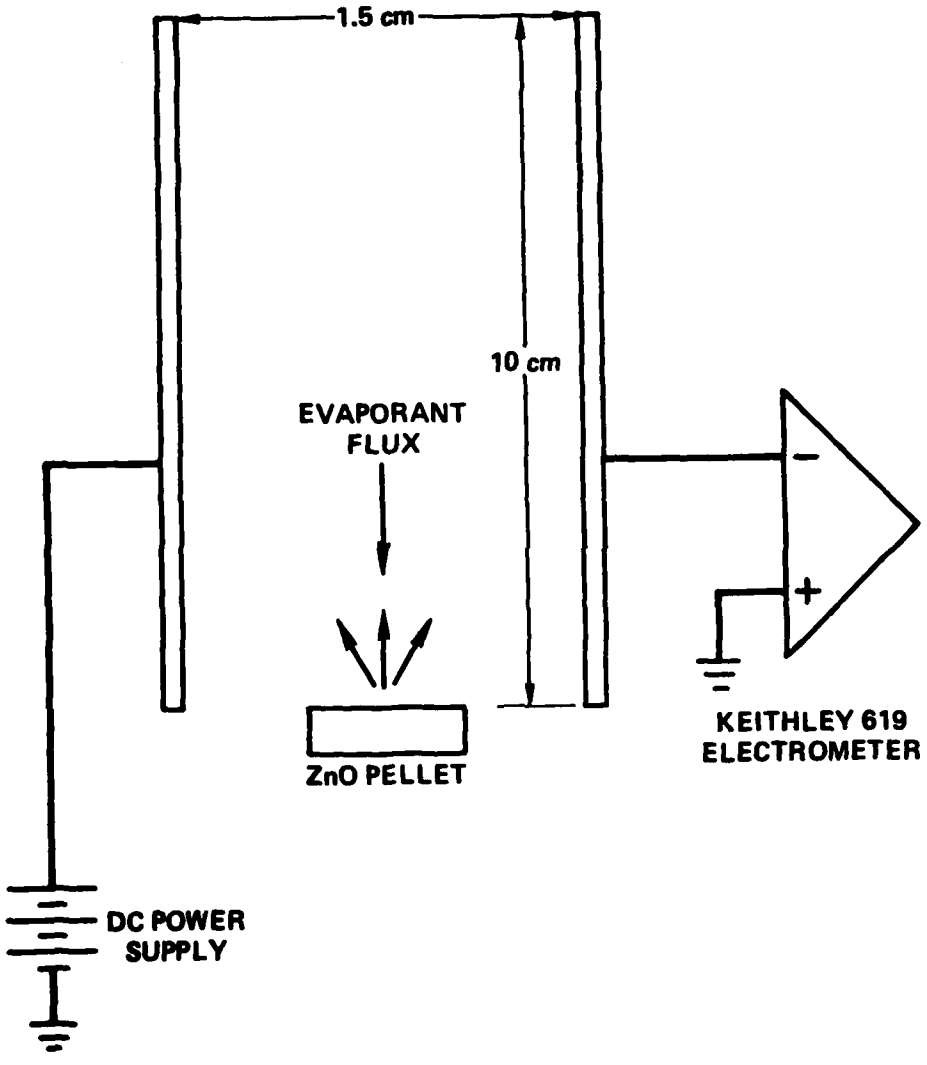

Fig. 24 Experimental setup to measure ionization duration laser evaporation of ZnO.

for which the heat of reaction ΔH = 083 kcal/mole. If the oxidizing agent is N_2O or O_2, the energy of reaction is even more negative.

Zn atoms encountered few O_2 atoms, if any, during their transit from the source to the substrate in vacuum. However, the growth surface is bombarded by O_2 molecules at the rate predicted by kinetic gas theory. The Zn concentration on the surface is given by the arrival rate and re-evaporation rate of Zn atoms. At growth temperatures higher than 200°C, the re-evaporation rate of Zn becomes comparable in order of magnitude to the impingement rate from the source for a range of laser power levels used. In fact, at 200°C, the vapor pressure of Zn over solid Zn is $p_{Zn} \simeq 10^{-5}$ Torr, hence evaporation rate, R_e

$$R_e = 44 \frac{M_{Zn}}{T} P(Zn) \times 10^{15} \text{ atoms/cm}^2\text{-s} \quad .$$

This corresponds to a few monolayer/s. The complete oxidation depends on the reaction kinetics and the Zn and O_2 concentration on the surface. If the ZnO evaporation rate is too rapid or if the re-evaporation of Zn from the substrate surface is slow, as is the case at low substrate temperatures, the film grows Zn rich and will consist mostly of Zn or of Zn particles in ZnO matrix. In the case of Au substrates, the oxidation kinetics seems to be slowed, possibly due to alloying of Zn with Au.

3.3.3 Optimization of ZnO Film Growth and Film Properties

Highly oriented polycrystalline ZnO films were grown on various substrates in vacuum pressures of 10^{-7}-10^{-3} on substrates held at temperatures of 100°-400°C. The evaporation rate was 0.1-10Å/s. These films were characterized by x-ray diffraction for their structural properties, by ellipsometry, reflectance and transmittance spectroscopy for their optical properties, by SAW transducers for their piezoelectric properties. These properties and the effect of growth conditions on these properties are discussed below.

3.3.3.1 Effects of Substrate

The crystallinity was found to be substrate dependent. The crystallinity was measured by x-ray diffraction (XRD) line peak height normalized by the thickness of the film.

For all substrates used, (0002) peak was the only x-ray diffraction line observed, indicating that the c-direction was normal to the substrate when the growth temperature was 250°C (Fig. 25). Sapphire, Si(100), Si(111), and Au(111) films used as substrates produced films with higher XRD counts. GaAs, quartz, and thermal SiO_2 substrates produced films with lower crystallinity. The high crystallinity of films on c-sapphire is explained by the epitaxial growth of ZnO. However, there is no epitaxial relationship between ZnO and other substrates. The difference in crystallinity between different substrates is attributed to differences of adatom mobility. The fact that x-ray counts of films grown on quartz and thermal SiO_2 on Si are different also point out to the above conclusion. The film on Au substrates, where adatom mobility is expected to be highest, produced films with highest x-ray count.

3.3.3.2 Structural Properties and the Effects of Temperature

The substrate temperature was found to have a strong effect on the growth rate, optical, and crystalline properties of ZnO films. Experiments were conducted with growth temperatures ranging from 25-450°C. In general, crystallinity increased (Fig. 26) and growth rate decreased with temperature. Temperature range for best crystalline structure was found to be 250-400°C. The increase in crystallinity is due to higher mobility of atoms, and the lower growth rate is thought to be due to re-evaporation of Zn atoms from the substrate surface or equivalently due to lowering the sticking coefficient of Zn.

Deposition on substrates at room temperature produced hard, glossy, black polycrystalline films. The transmittance and reflectivity spectra of these are shown in Fig. 27. The films are highly absorbing in the UV and visible range due to Zn precipitates. The polycrystals are not totally

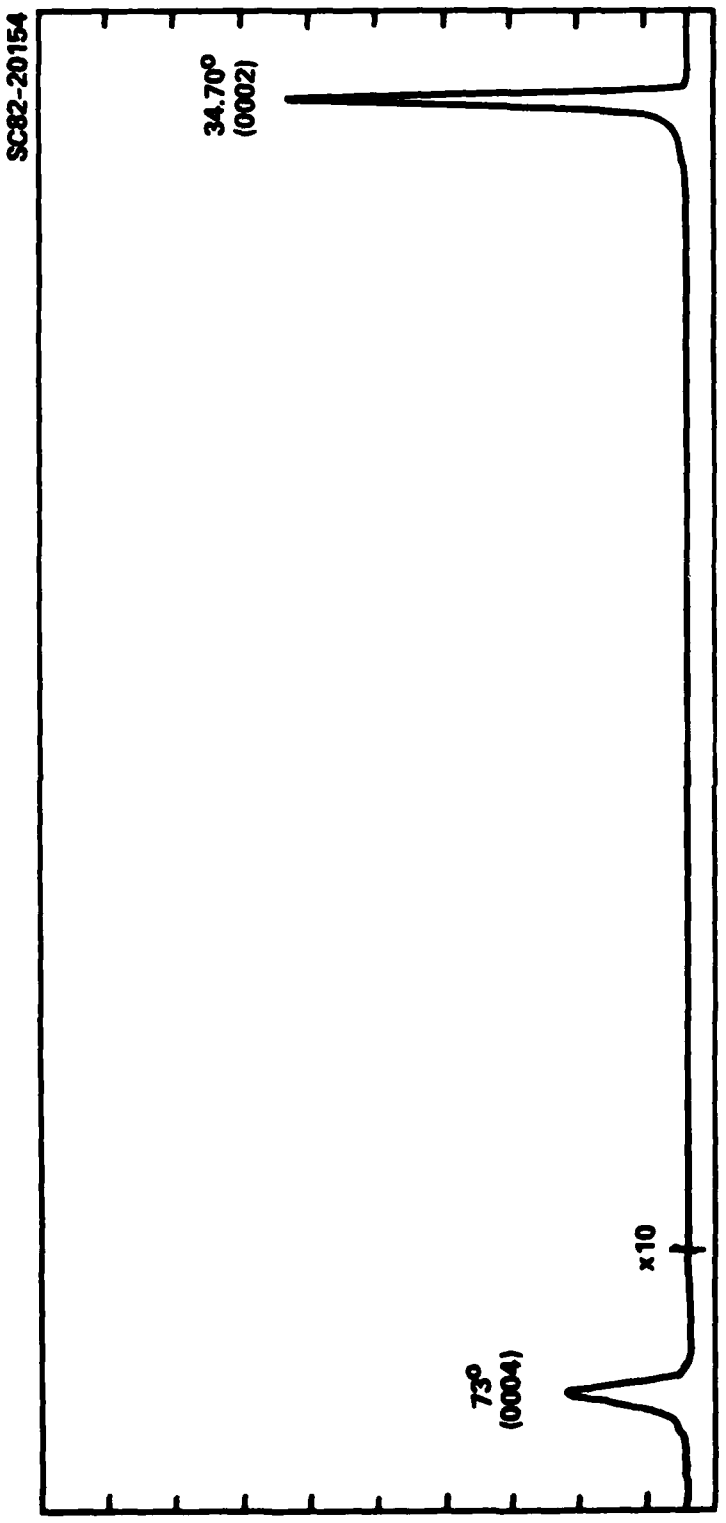

Fig. 25 X-ray diffraction spectrum of LADA ZnO film on Si substrated at 250°C.

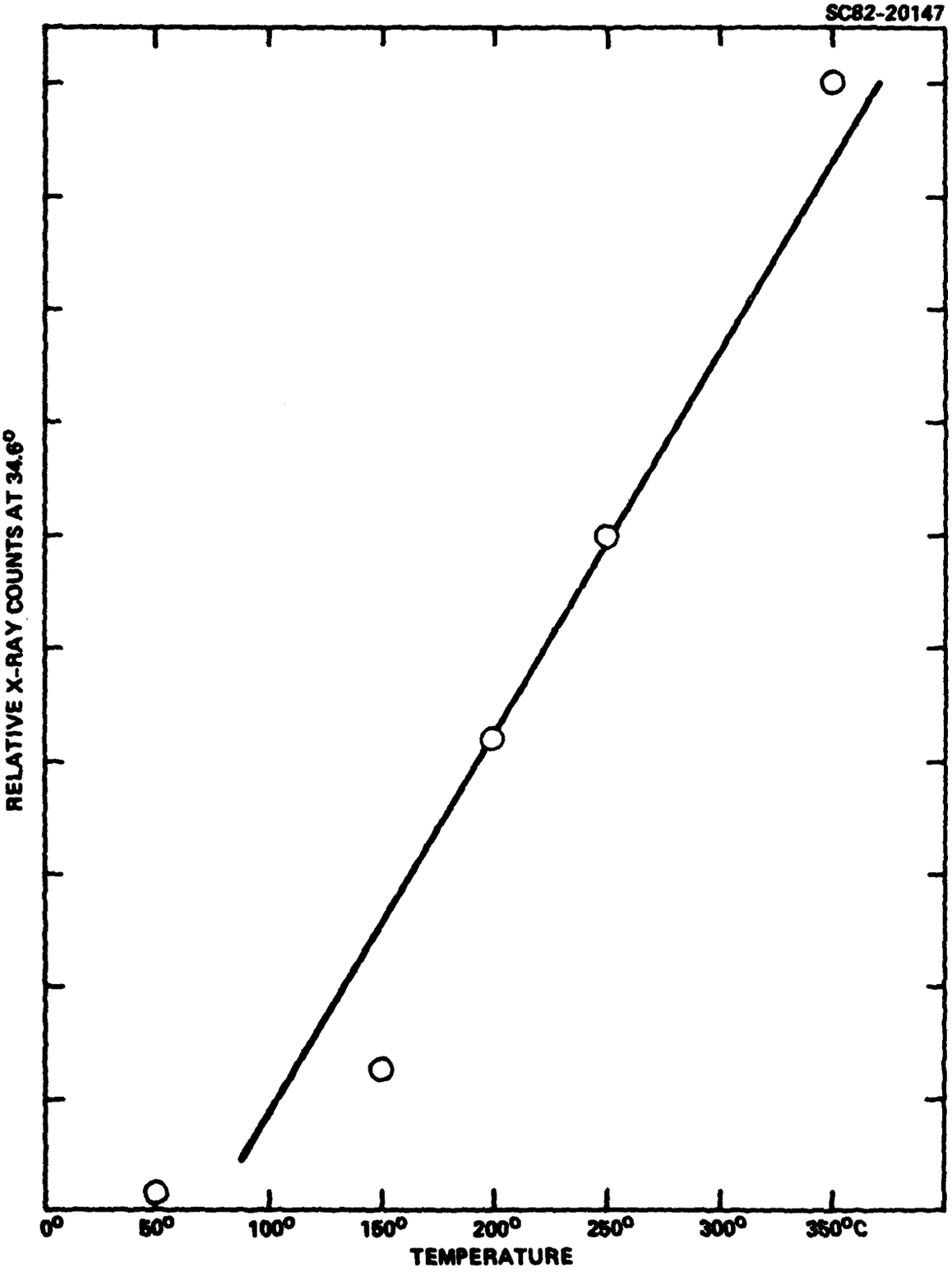

Fig. 26 Crystallinity vs growth temperature.

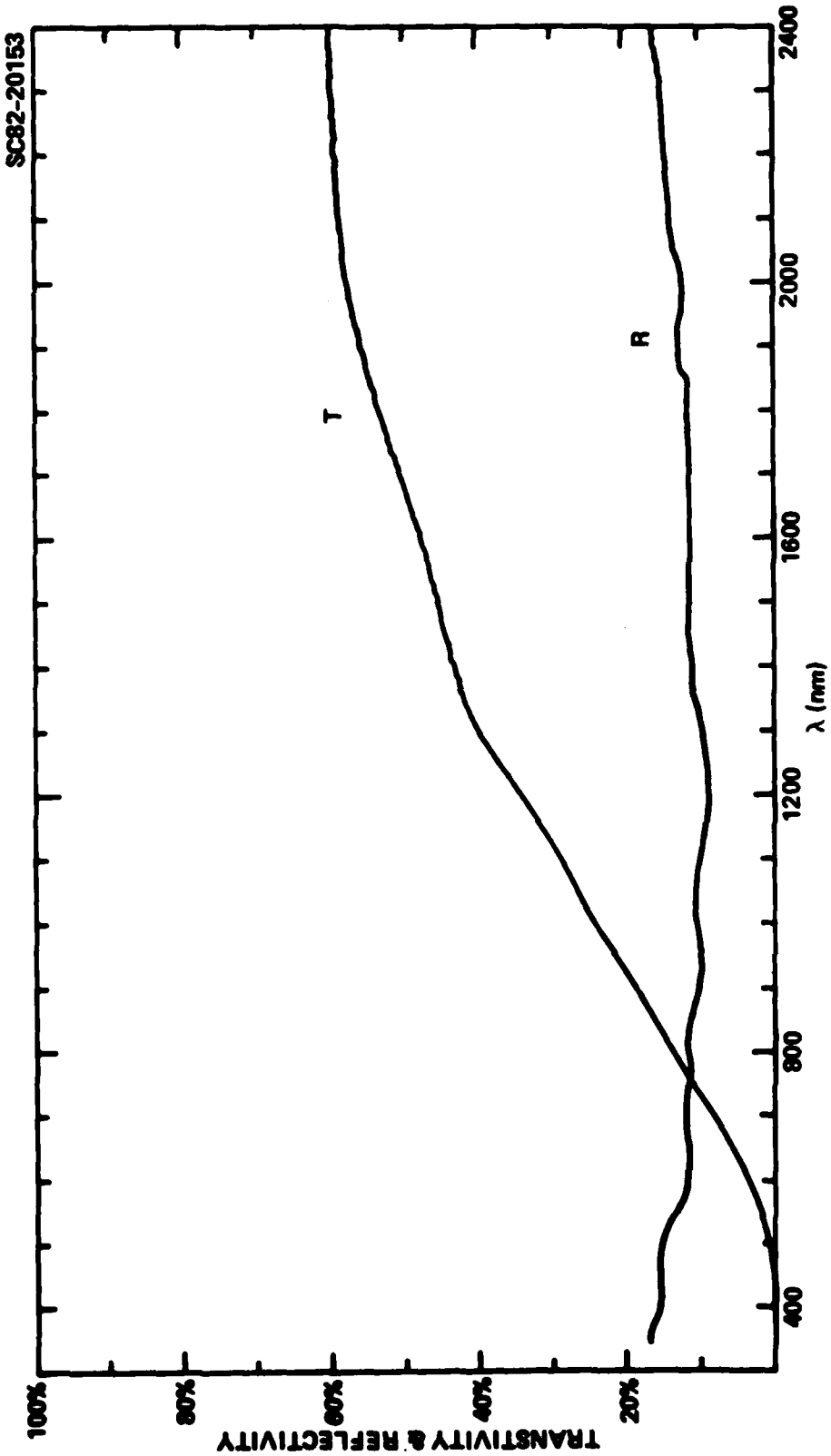

Fig. 27 Transmission and reflection spectra of a LADA ZnO film on quartz substrate grown at room temperature.

oriented, but (0002) XRD line is still the strongest peak. These films are truly ZnO as indicated by x-ray diffraction, as well as by ESCA measurements. Free Zn is not observed by either technique, although the black color of the films and the growth conditions indicate that Zn clusters or precipitates must exist in the bulk of the film.

Optically clear, highly crystalline and oriented films were produced at temperatures higher than 100-200°C. The lower temperature found for good quality films is affected by the evaporation rate as is explained in previous paragraphs. In general, the films grown at temperatures higher than 400°C had lower crystallinity than films grown at 400°C.

3.3.3.3 Optical Properties

Transmission and reflectivity spectra for 1 μm film grown on quartz are shown in Fig. 28. The presence of interference maxima and minima indicates the uniform nature of the films. The refractive index values obtained from the position of the maxima and minima using the formula

$$n = \frac{1}{2t} \frac{\lambda_1 \lambda_2}{\lambda_1 - \lambda_2}$$

where t is the thickness and λ's are any adjacent maxima or minima, were found to be in close agreement with those obtained from ellipsometric measurements in the same films and refractive index values of best films obtained by RF sputtering as reported in literature.[17]

Samples grown on transparent quartz substrates were investigated optically by using polarizing plates under a microscope. This was to observe the orientation of grains utilizing the birefringent nature of ZnO. The samples appeared uniform, indicating that the grains were either too small so that any optical nonuniformities averaged out, or that the layer was nearly single crystal or an aggregate or crystallities similarly oriented in azimuthal

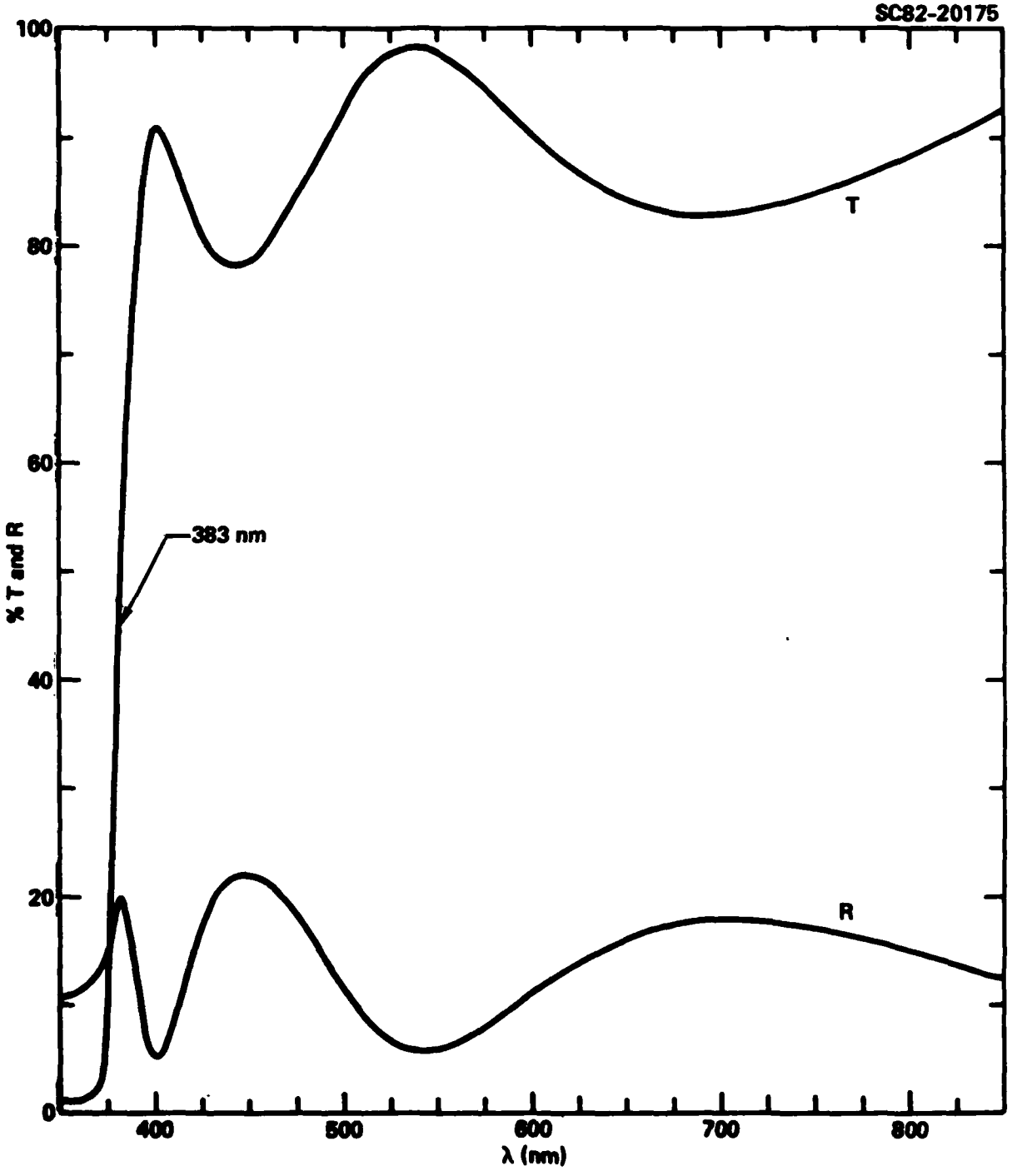

Fig. 28 Transmission and reflection spectra of a LADA ZnO film grown on quartz at 250°C.

direction. Laue backreflection results favor the model of oriented polycrystallites aggregate.

3.3.3.4 Electrical Properties and Effect of Annealing

As-grown samples were found to be conducting with resistivity in the 0.1-1 Ω-cm range, as measured with van der Pauw method. Isothermal annealing in air or in oxygen at temperatures of 250-700°C and pressures of 0.2-100 kg/cm^2 produced nonconducting films in the direction parallel to the film surface, but not across the film. This is thought to be due to the diffusion of oxygen along boundaries of columnar grains and the consequent increase of the potential barrier across the boundaries.[18] Thus, the conductivity parallel to the surface decreases, whereas the conductivity in the direction normal to the surface is dominated by the bulk conductivity through the grains; thus it remains high.

3.3.3.5 Effect of Li Doping

The effect of Li doping on crystallinity and conductivity was investigated as a function of Li concentration in the source material. Li is known to compensate for native donors in ZnO.

In the initial set of experiments Li_2CO_3 powder was mixed with ZnO by ball milling. The Li to Zn ratio in the source varied from 4%, 2%, 1%, 5%, 0.2%. The films grown with 1% or higher Li concentration were nonconducting, but had low or no crystalline structure. The films with low crystalline structure were under nonuniform stress as indicated by the high XRD line width and long trailing edge of the high angle side of the (0002) line.[9] Furthermore, the films were sensitive to ambient moisture and were observed to slowly deteriorate in room air. This is thought to be due to the excess Li in the films forming a basic solution with moisture in the environment, which then dissolves ZnO because of the latter's amphoteric nature. In fact, the LnO:Li films were found to be water soluble and if left in DI water over a period of time, completely dissolved away. In another set of experiments, a water solution of $Li_2O \cdot H_2O$ was mixed with ZnO powder and the resulting sludge dried

in vacuum. Since Li atoms are expected to be adsorbed on the surface of ZnO particles, it is expected that this technique would render a more uniform distribution of Li throughout the source material. This technique also allowed smaller amounts of the dopant to be used. The atomic Li concentration in the source varied from 1%-0.1%. Films thus obtained were found to be nonconducting in the direction parallel and perpendicular to the film surface, but also to have excellent crystallinity. These were neither susceptible to ambient moisture nor dissolved in DI water. X-ray diffraction spectrum indicated that the films were stress free. The minimum amount of Li necessary to render the films highly resistive has not yet been determined. It is expected that further improvement in film quality will result when Li doping concentration is reduced.

3.3.3.6 Effect of O_2 Glow Discharge

Several LADA ZnO runs were made in a O_2 glow discharge environment. The O_2 pressure was held at 10 μm and ac glow discharge was obtained by means of high voltage electrical leads. The resulting films were transparent, had high resistivity, but poor crystallinity. The active O_2 in ionized or excited form is thought to completely oxidize the Zn atoms on the growth surface, thus eliminating free interstitial Zn that act as shallow donors. The poor crystallinity, on the other hand, suggest the possibility of very small crystallites with potential barriers on their surfaces as the physical cause of high resistivity. Due to structural characteristics, we will use Li doped ZnO for high resistivity samples.

3.3.3.7 Effect of Gas in the Vacuum System

Most experiments have been carried out either in vacuum or in O_2 atmosphere at pressures of 5×10^{-4}, 1×10^{-3} and 1×10^{-2} Torr. No difference in optical, crystalline, or electrical properties were observed in ZnO grown on quartz, Si, or sapphire when the growth environment was hard vacuum (10^{-6} Torr) or O_2 gas at $5 \sim 10^{-4}$ Torr pressure or higher. The above indicates that re-evaporation or oxidation kinetics is substrate dependent. Zn atoms on Au are

slow to re-evaporate or to oxidize, thus becoming buried under new layers of Zn and ZnO. This behavior is specific to Au and is not seen on Ti films. A possible explanation lies in the fact that Au and Zn form continuous alloys with 3 ordered phases (Fig. 29). The alloying of Zn on the surface may slow its oxidation because the solute Zn in low concentrations will behave somewhat like the solvent Au. Careful x-ray analysis did not show presence of Au_3Zn, AuZn or $AuZn_3$ compounds at the interference of ZnO and Au films.

Films grown in O_2 concentrations of $1\text{-}2 \times 10^{-2}$ Torr on any substrate showed poor crystallinity and low resistivity. It is to be noted that 10^{-2} Torr O_2 pressure with glow discharge gave films with equally poor crystallinity, but very high resistivity and high breakdown voltage.

3.3.3.8 Effect of Annealing

Isothermal annealing affects optical, electrical, and crystalline properties of films. In general, crystallinity improved with annealing temperatures of 250-400°C and with annealing time within 2 hours. However, when film structure was so disordered that no crystallinity order existed, annealing does not improve crystallinity. Isothermal annealing at 250°C in flowing O_2 for 8 hours hardened the films, eliminating low breakdown regions. Annealing at higher temperature (400-700°C) changed the black-glossy films grown at room temperature to transparent or translucent films, possibly by dissolving or oxidizing Zn clusters that give rise to the dark color of the films. The activation energy for the crystallite growth during annealing was found to be 0.15 eV.

3.3.3.9 Piezoelectrical Response

Although ZnO has the highest piezoelectric coupling coefficient among the II-VI compounds, thus far only ZnO films produced by sputtering exhibit this property. In fact, ZnO by magnetron sputtering is considered as the state-of-the-art and is regarded as the baseline material for fabricating surface acoustic wave (SAW) devices. ZnO films produced by LADA technique are also

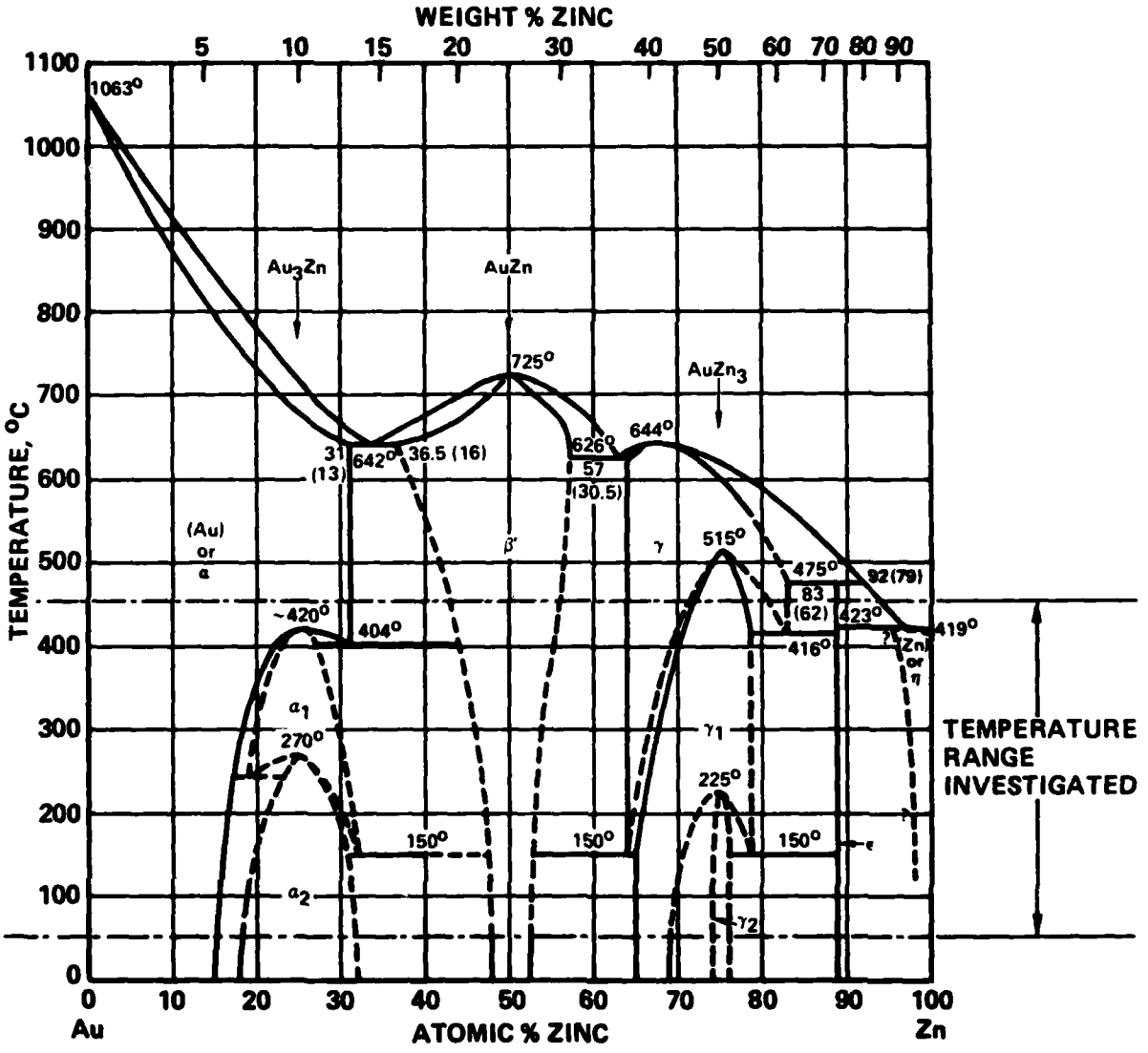

Fig. 29 Phase diagram of Au-Zn system.

piezoelectric. We have successfully demonstrated SAW transducers fabricated on 4000A LADA ZnO films deposited on silicon and fused quartz substrates. Fabrication and characterization of these devices were performed by D.E. Motamedi at Rockwell's Microelectronics Research and Development Center.

To characterize the acoustic response of ZnO film evaporated by laser assisted technique, SAW transducers were designed for a resonant frequency of 328 MHz using a $ZnO/SiO_2/Si$ overlay structure. The transducers had an acoustic wavelength of approximately 12 μm and finger overlapping of W = 50 wavelengths. Several transducers with different numbers of finger-pairs are contained in each chip to best characterize the frequency response of the device. The interdigital electrode array is located on the top surface with a metal conductive film directly located under the electrodes at the interface. The thickness of ZnO in this configuration is chosen for the first peak of $\Delta V/V$ curve. Silicon substrate is (111) with a resistivity of 5-10 ohm-cm.

The complex return loss of the device is plotted by HP 8505 Network Analyzer and HP 8501 storage normalizer. The result is shown in Fig. 30. Using the technique reported previously,[4] we found the ZnO film has a coupling coefficient of $K^2 = 0.005$. Considering the reported theoretical value of $K^2 = 0.010$, we believe this result is excellent for the first reported SAW transduction of piezoelectric ZnO films using laser assisted evaporation techniques.

Shown in Fig. 31 is a plot of acoustic signal transmission (amplitude of S_{21}) between two interdigital transducers spaced for 2.6 μs of delay. The total insertion loss (untuned) is 35 dB at the center frequency of 328 MHz. No attempt is made at this stage for the best shielding and reducing the cross-talks which is responsible for the poor isolation at the high frequency response. The amplitude of the return loss is also plotted in this figure to show the correlation of the high frequency roll off.

Fabrication of interdigital transducers with the same configuration on fused quartz substrate produced similar results. The center frequency was reduced to 240 MHz and the value of $K^2 = 0.004$ was slightly smaller than K^2 achieved for silicon substrates.

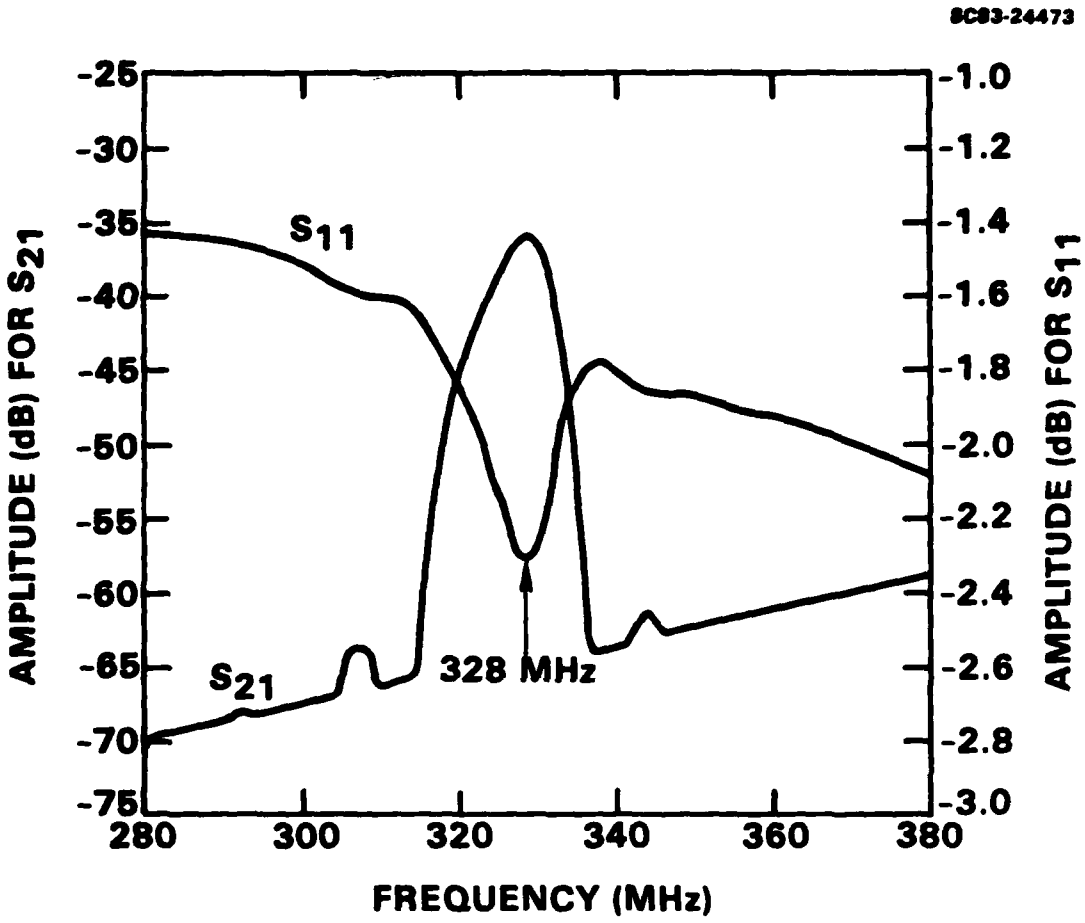

Fig. 30 Frequency response of 328 MHz SAW transducer generated by HP 8595 Network Analyzer. Substrate is thermally oxidized silicon which is overlayed by 4000A of laser evaporated ZnO. Interdigital transducers have 20 finger-pairs spaced for 2.6 μs of delay. The total insertion loss is 35 dB when transducers are untuned.

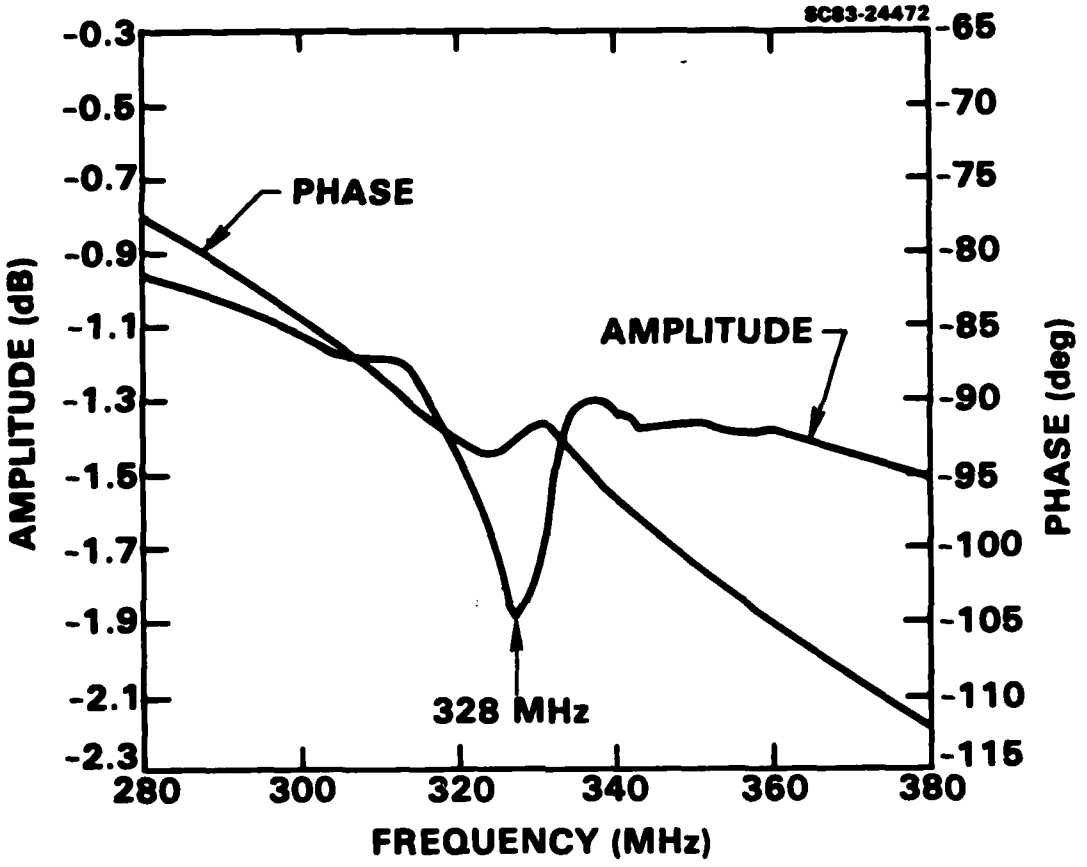

Fig. 31 Phase and amplitude of complex return loss (S_{11}) of a SAW transducer built on LADA ZnO over thermally oxidized Si.

4.0 SUMMARY

In this program, we have developed a novel technique (LADA) for thin film growth. Semiconductors (HgCdTe and CdTe) and a dielectric (ZnO) have been successfully grown. In some cases, the properties of these materials compares favorably with those from well-developed conventional methods.

Epitaxial $Hg_{0.7}Cd_{0.3}Te$ layers were grown on CdTe at very low substrate temperature from an evaporation source. This is the result of congruent evaporation conditions unique to LADA. The layer quality is strongly dependent on the laser conditions. Converting the as-grown n-type layer to p-type by annealing has been demonstrated.

Heteroepitaxy of CdTe on GaAs was also successful. We were able to grow (111)CdTe over (111)GaAs substrate. The layers were characterized by x-ray, UV reflectance, photoluminescence and transmission electron microscopy (TEM). Results indicate their crystallinity quality comparable to bulk CdTe.

In the area of ZnO, we were able to deposit SAW device films on various substrates at 250°C which is much lower than the substrate temperature used by the state-of-the-art magnetron sputtering. The piezoelectric nature of the LADA ZnO films was demonstrated by SAW transducer measurements.

Throughout this program, we have learned and developed this technique in both its engineering and scientific aspects. The hardware has been through stages of redesign and modification to make routine operation feasible and reliable. Scientifically, we have gained some insights on the mechanism of pulsed laser induced evaporation and its advantage of the more conventional methods. There are many unique advantages. It is clean (crucibleless), simple and flexible (laser unit locates external to the vacuum chamber). The response in controlling the evaporation rate is instantaneous. The evaporation is congruent and dissociative. Under high laser power, the evaporation can also produce high energy (1-5 eV) neutral species, fraction of ions, and an intense UV radiation. All of these features are believed to enhance the film qualities. Only a few have been applied to the materials studied

here. This area has a lot of potential for future development to produce thin films which no other current methods are capable of. A logical extension of this work will be growth of HgCdTe/CdTe/GaAs structures, and further refinement of ZnO growth. Pyroelectric materials are also ideal candidates. Meanwhile, a continuous basic study on the evaporation/deposition mechanism of LADA and their implications to material application is also needed in order to fully exploit all advantages.

SC5202.23FR

5.0 PUBLICATION LIST

Publications Under This Contract

1. "Growth of HgCdTe Films by Laser Induced Evaporation and Deposition," J.T. Cheung and D.T. Cheung, J. Vac. Sci. Tech. 21(1), 182 (1982).

2. "Epitaxial Growth of $Hg_{0.7}Cd_{0.3}Te$ by Laser Assisted Deposition," J.T. Chueng, Appl. Phys. Lett. 43(3), 255 (1983).

3. "Heteroepitaxial Growth of CdTe on GaAs by Laser Assisted Deposition," J.T. Cheung, M. Khoshnevisan and T. Magee, Appl. Phys. Lett. 43(5), 462 (1983).

4. "Recent Progress on LADA Growth of HgCdTe and CdTe Epitaxial Layers," J.T. Cheung and T. Magee, J. Vac. Sci. Tech. A1(3), 1604 (1983).

5. "Highly Oriented ZnO Films by Laser Assisted Deposition," H. Sankur and J.T. Cheung, J. Vac. Sci. Tech. November-December (1983).

6. "Properties of ZnO Thin Films by Laser Evaporation," H. Sankur and E. Motamedi, Proceeding IEEE Ultrasonic Symposium, Atlanta, GA, November 1983.

7. "Mechanism of Laser-Assisted Evaporation of II-VI Semiconductors and its Application to Thin Film Growth," J.T. Cheung, MRS Proceeding on Laser Controlled Chemical Processing of Surface, Boston, Mass. November 1983.

Related Publications

1. "Properties of Dielectric Thin Films Formed by Laser Evaporation," H. Sankur, MRS Proceeding on Laser Controlled Chemical Processing of Surfaces, Boston, Mass. November 1983.

2. "Logarithmic Behavior in a New Two-Dimensional Metal: HgTe-CdTe Superlattice," N.P. Ong, G. Kote and J.T. Cheung, Phys. Rev. B, 28(4), 2289 (1983).

6.0 REFERENCES

1. H. Schwartz and H.A. Tourlellot, J. Vac. Sci. Tech. 6, 373 (1969); A. Stephens, T.J. Zrebiec and V.S. Ban, Mat. Res. Bull. 9, 1427 (1974); Yu.A. Bykoviskii, et al, Soviet Phys. Tech. 23(5), 1978.

2. J.T. Cheung and D.T. Cheung, J. Vac. Sci. Tech. 21, 182 (1982).

3. J.T. Cheung, Appl. Phys. Lett. 43, 255 (1983).

4. J.T. Cheung, M. Khoshnevisan and T. Magee, Appl. Phys. Lett. 43, 412 (1983).

5. G. Calli and J.E. Coker, Appl. Phys. Lett. 16, 439 (1970).

6. C.K. Lau, S.K. Tiku and K.M. Lakin, J. Elec. Chem. Soc. 127, 1843 (1980).

7. R.F. Belt and G.G. Florio, J. Appl. Phys. 39, 5215 (1968).

8. B.T. Khuri-Yakub, J.G. Swits and T. Barbee, J. Appl. Phys. 52, 4772 (1982).

9. H. Sankur and J.T. Cheung, J. Vac. Sci. Tech. (to be published in October-December 1983).

10. V. Canevari, U. Emiliani, N. Romero and G. Sberveglieri, Thin Solid Films, 106, L91 (1983).

11. A.R. Calawa, Appl. Phys. Lett. 38, 701 (1981).

12. G.P. Schwartz, V.E. Bondebly, J.H. English and G.H. Gualtieri, Appl. Phys. Lett. 42, 952 (1983).

13. J.P. Faurie, A. Million and H.G. Jacquier, Thin Solid Films, 90, 107 (1982).

14. N.P. Ong, G. Kote and J.T. Cheung, Phys. Rev. B.

15. S. Iida and K. Ito, J. Electrochem. Soc. 118, 768 (1971).

16. T.H. Myers, S.W. Edwards and J.F. Schetzina, J. Appl. Phys. 53, 4231 (1981).

17. J.R. Shealy et al, J. Electrochem Soc. 128, 558 (1981).

18. J.C. Yen, J. Vac. Sci. Tech. 12, 47 (1975).

19. M. Mhijra, Jap. J. Appl. Phys. 21, 264 (1982).